A rationally designed peptidomimetic modulator of CaV2.2 (N-type) voltage-gated calcium channels for chronic pain

Kimberly Gomez[1], Ulises Santiago[2], Paz Duran[1], Yuan Zhou[3], Aida Calderon[1], Santiago Loya-López[1], Angie Dorame[4], Aude Chefdeville[3], Aubin Moutal[4], Dongzhi Ran[4], Samantha Perez-Miller[3], Yi Lu[5], Xia Liu[5], Handoko Handoko[1], Paramjit Arora[1], Marcel Patek[6], Carlos J. Camacho[2], and Rajesh Khanna[1]

[1]New York University
[2]University of Pittsburgh
[3]University of Arizona
[4]University of Arizona Medical Center - University Campus
[5]Chongqing Medical University
[6]Bright Rock Path LLC

September 12, 2022

Abstract

Background and Purpose Transmembrane Cav2.2 (N-type) voltage-gated calcium channels are genetically and pharmacologically validated pain targets. Clinical block of Cav2.2 (e.g., with Prialt) or indirect modulation (e.g., with gabapentinoids) mitigates chronic pain but is constrained by side effects. The cytosolic auxiliary subunit collapsin response mediator protein 2 (CRMP2) targets Cav2.2 to the sensory neuron membrane and regulates their function. A CRMP2-derived peptide (CBD3) uncouples the Cav2.2-CRMP2 interaction to inhibit calcium influx, transmitter release and pain. Homology-guided mutagenesis of CBD3 revealed an antinociceptive core at A1RSR4. Here, the A1R2 CBD3 dipeptide was identified as critical for Cav2.2 molecular recognition and served as a scaffold for identification of small molecule peptidomimetic allosteric regulators of Cav2.2. Experimental Approach We developed and applied a novel molecular dynamics approach to identify the Cav2.2 recognition motif of the core CBD3 peptide as the A1R2 dipeptide and used its presenting motif to design pharmacophore models to screen 27 million compounds in the open access server ZincPharmer. Of 200 curated hits, 77 compounds were assessed using depolarization-evoked calcium influx in rat dorsal root ganglion (DRG) neurons. Nine compounds were tested using electrophysiology and one compound (CBD3063) was evaluated biochemically, electrophysiologically, and behaviorally effects in a model of experimental pain: Key Results CBD3063 reduced membrane Cav2.2 expression and currents, inhibited neuronal excitability, uncoupled the Cav2.2-CRMP2 interaction, and reversed mechanical allodynia in rats with spared nerve injury. Conclusions and Implications These results identify CBD3063, as a selective, first-in-class, CRMP2-based peptidomimetic, which allosterically regulates Cav2.2 to achieve analgesia.

A rationally designed selective peptidomimetic modulator of $Ca_V2.2$ (N-type) voltage-gated calcium channels for chronic pain

Kimberly Gomez[1,2+], Ulises Santiago[3+], Aida Calderon-Rivera[1,2], Paz Duran[1,2], Santiago Loya-Lopez[1,2], Angie Dorame[4], Aude Chefdeville[4], Aubin Moutal[4], Dongzhi Ran[5], Samantha Perez-Miller[1,2], Yi Lu[5], Xia Liu[5], Handoko[6], Paramjit S. Arora[6], Marcel Patek[7], Carlos J. Camacho[3,*], and Rajesh Khanna[1,2,*]

[1]Department of Molecular Pathobiology, College of Dentistry, New York University, 433 First Avenue, 8thfloor, New York, NY, 10010, USA.

[2]NYU Pain Research Center, 433 First Avenue, New York, NY 10010, USA.

[3]Department of Computational and Systems Biology, University of Pittsburgh, Pittsburgh, PA, 15261, USA.

[4]Department of Pharmacology, College of Medicine, University of Arizona, Tucson, AZ 85724, USA.

[5]Department of Pharmacology, School of Pharmacy, Chongqing Medical University, Chongqing 400016, China

[6]Department of Chemistry, New York University, 100 Washington Square East, New York, NY 10003, USA.

[7]Bright Rock Path LLC, Tucson, Arizona, USA.

[+]Contributed equally to this work

*Correspondence to:

Dr. Carlos J. Camacho, Department of Computational and Systems Biology, University of Pittsburgh, Pittsburgh, PA, 15261, USA. Email:*ccamacho@pitt.edu* or

Dr. Rajesh Khanna, Department of Molecular Pathobiology, College of Dentistry, New York University, 433 First Avenue, 8$^{\text{Th}}$floor, New York, NY, 10010, USA. Office phone: (520) 271-0433; Email:*rk4272@nyu.edu*

Data Availability Statement: The data that support the findings of this study are available from the corresponding author upon reasonable request. Some data may not be made available because of privacy or ethical restrictions.

What is already known

$Ca_v2.2$(N-type) voltage-gated calcium channels contribute to neuronal excitability and neurotransmission.

The auxiliary subunit collapsin response mediator protein 2 (CRMP2), allosterically modulates $Ca_v2.2$.

What this study adds

A CRMP2-derived peptide (CBD3) uncouples the $Ca_v2.2$-CRMP2 interaction to inhibit calcium influx, neurotransmission, and pain.

The peptidomimetic CBD3063 blocks $Ca_v2.2$ activity, uncouples the $Ca_v2.2$-CRMP2 interaction, and reverses neuropathic pain.

Clinical significance

CBD3063 is a first-in-class, CRMP2-based peptidomimetic, which selectively regulates $Ca_v2.2$ to achieve analgesia.

A biophysical-based computational pipeline may yield additional active chemotypes responsible for CBD3's interaction with $Ca_v2.2$.

Abstract

Background and Purpose

Transmembrane $Ca_v2.2$ (N-type) voltage-gated calcium channels are genetically and pharmacologically validated pain targets. Clinical block of $Ca_v2.2$ (e.g., with Prialt) or indirect modulation (e.g., with gabapentinoids) mitigates chronic pain but is constrained by side effects. The cytosolic auxiliary subunit collapsin response mediator protein 2 (CRMP2) targets $Ca_v2.2$ to the sensory neuron membrane and regulates their function. A CRMP2-derived peptide (CBD3) uncouples the $Ca_v2.2$-CRMP2 interaction to inhibit calcium influx, transmitter release and pain. Homology-guided mutagenesis of CBD3 revealed an antinociceptive core at A_1RSR_4. Here, the A_1R_2 CBD3 dipeptide was identified as critical for $Ca_v2.2$ molecular recognition and served as a scaffold for identification of small molecule peptidomimetic allosteric regulators of $Ca_v2.2$.

Experimental Approach

We developed and applied a novel molecular dynamics approach to identify the $Ca_v2.2$ recognition motif of the core CBD3 peptide as the A_1R_2 dipeptide and used its presenting motif to design pharmacophore models to screen 27 million compounds in the open access server ZincPharmer. Of 200 curated hits, 77 compounds were assessed using depolarization-evoked calcium influx in rat dorsal root ganglion (DRG) neurons. Nine compounds were tested using electrophysiology and one compound (CBD3063) was evaluated biochemically, electrophysiologically, and behaviorally effects in a model of experimental pain:

Key Results

CBD3063 reduced membrane $Ca_v2.2$ expression and currents, inhibited neuronal excitability, uncoupled the $Ca_v2.2$-CRMP2 interaction, and reversed mechanical allodynia in rats with spared nerve injury.

Conclusions and Implications

These results identify CBD3063, as a selective, first-in-class, CRMP2-based peptidomimetic, which allosterically regulates $Ca_v2.2$ to achieve analgesia.

Keywords: $Ca_v2.2$, CRMP2, Peptidomimetics, Molecular Dynamics Simulations, Chronic Pain.

Introduction

In the central and peripheral nervous systems, transmembrane $Ca_v2.2$ (N-type) voltage-gated calcium channels are expressed in the dorsal root ganglia (DRG) and spinal dorsal horn (SDH) – two important sites for nociceptive transmission (Hoppanova & Lacinova, 2022). Within the spinal cord, $Ca_v2.2$ channels are localized in the central terminals of primary afferent fibers where they mediate the release of excitatory neurotransmitters (Heinke, Balzer & Sandkuhler, 2004). Knockout mouse models of $Ca_v2.2$ (Hatakeyama et al., 2001; Kim et al., 2001) demonstrated a key role for these channels in nociceptive pathways: $Ca_V2.2$ deficient mice show reduced response to mechanical stimuli in the von Frey test and increased tail flick latency in response to radiant heat, indicating altered spinal reflexes (Irwin, Houde, Bennett, Hendershot & Seevers, 1951); however, in the hot plate test, which is an assay of supraspinal nociceptive integration (Giglio, Defino, da-Silva, de-Souza & Del Bel, 2006), pain responses are unaltered (Kim et al., 2001). That expression and function of $Ca_v2.2$ channels increases following nerve injury (Cizkova et al., 2002; Yang et al., 2018; Yu et al., 2019b) demonstrates plasticity of this target for therapeutic intervention.

Three drugs targeting $Ca_v2.2$ channels are commercially available for management of neuropathic pain conditions. Ziconotide (Prialt®) – a synthetic version of the cone snail toxin ω-conotoxin MVIIA – is a $Ca_v2.2$ channel blocker and was the first non-opioid intrathecal analgesic approved by the US Food and Drug Administration for the treatment of intractable chronic pain (Doggrell, 2004). Its use is hampered by its invasive route of administration, narrow therapeutic window, and a panoply of side effects. Gabapentin (Neurontin®) and Pregabalin (Lyrica®) – ligands of α2δ-1 auxiliary subunit of $Ca_v2.2$ channels – alleviate chronic pain by disrupting $Ca_v2.2$ –α2δ-1 interaction to prevent $Ca_v2.2$ trafficking to the plasma membrane (Bauer, Rahman, Tran-van-Minh, Lujan, Dickenson & Dolphin, 2010; Hendrich et al., 2008; Sutton, Martin, Pinnock, Lee & Scott, 2002). Both gabapentinoids have low efficacy and present with serious side effects (Evoy, Peckham, Covvey & Tidgewell, 2021). Misuse of gabapentinoids has led to an increase in overdose-related deaths between 2019 and 2020 (Kuehn, 2022). Therefore, there is a critical need to develop novel medicines that effectively manage pain without producing negative side effects.

Alternative approaches have been devised to regulate the functional activity of $Ca_v2.2$ channels by targeting proteins that interact with them. In this regard, we identified collapsin response mediator protein 2 (CRMP2) as a regulator of $Ca_v2.2$ trafficking and function (Brittain, Piekarz, Wang, Kondo, Cummins & Khanna, 2009; Chi et al., 2009; Khanna et al., 2019). CRMP2 is a microtubule-binding protein that regulates neuronal polarity *in vitro* (Goshima, Nakamura, Strittmatter & Strittmatter, 1995; Inagaki et al., 2001). Importantly, CRMP2 interacts with $Ca_v2.2$ (Brittain, Piekarz, Wang, Kondo, Cummins & Khanna, 2009; Khanna, Zougman & Stanley, 2007). Overexpression of CRMP2 leads to enhanced $Ca_v2.2$ currents and surface expression (Brittain, Piekarz, Wang, Kondo, Cummins & Khanna, 2009; Chi et al., 2009) and enhanced neurotransmitter release (Brittain, Piekarz, Wang, Kondo, Cummins & Khanna, 2009; Chi et al.,

2009) in hippocampal (Brittain, Piekarz, Wang, Kondo, Cummins & Khanna, 2009) and DRG neurons (Chi et al., 2009). A 15-amino-acid peptide (designated CBD3, for calcium channel binding domain 3) generated from CRMP2 interfered with the $Ca_v2.2$-CRMP2 protein-protein interaction and decreased calcium influx, transmitter release, and acute, inflammatory, and neuropathic pain (Brittain et al., 2011b). Homology-guided mutational analysis of CBD3 revealed an antinociceptive core in the first six amino acids with two residues (Ala_1 and Arg_4) accounting for most of the binding affinity (Moutal et al., 2018).

In the absence of any significant structural information on $Ca_v2.2$ to guide a rational design of small molecule inhibitors, we developed a novel pipeline that leverages molecular dynamics of the core peptide and identified the A_1R_2 dipeptide as the most stable conformational motif. Based on well-established biophysical principles (Rajamani, Thiel, Vajda & Camacho, 2004), we defined this motif to be the anchor of the interaction responsible for molecular recognition of $Ca_v2.2$. Thus, we used the A_1R_2 ensemble as scaffold to design pharmacophore models to predict first-in-class compounds to disrupt CRMP2-$Ca_v2.2$ interaction. Screening 27 million commercially available compounds led to the identification of a first-in-class peptidomimetic ((3R)-3-acetamido-N-[3-(pyridin-2-ylamino)propyl]piperidine-1-carboxamide; hereafter designated as CBD3063) that disrupted the $Ca_v2.2$-CRMP2 interaction, inhibited $Ca_v2.2$ function, and reversed experimental neuropathic pain.

Methods

Rational design of pharmacophore models in the absence of receptor structure.

Molecular dynamics of CBD3 peptide

We modeled the CBD3 peptide based on the X-ray diffraction structure of CRMP2 (PDB: 5MKV) (Zheng et al., 2018). Three independent molecular dynamics simulations (MDS) of both the CBD3 by itself and conjugated with a blood-brain barrier-permeable peptide TAT-CBD3 were run with pmemd.cuda (Case et al., 2018; Götz, Williamson, Xu, Poole, Le Grand & Walker, 2012; Salomon-Ferrer, Götz, Poole, Le Grand & Walker, 2013) from AMBER18 using AMBER ff14SB force field (Maier, Martinez, Kasavajhala, Wickstrom, Hauser & Simmerling, 2015). We used tLeap binary (AMBER18) for solvating the peptides in an octahedral TIP3P water box with a 15 Å distance from structure surface to the box edges, and closeness parameter of 0.75 Å. The neutralized system was solvated in a solution of 150 mM NaCl. H-bonds were constrained using SHAKE algorithm and integration time-step at 2 fs. Simulations were carried out equilibrating the system for 1 ns at NPT using Berstein barostat to keep constant pressure at 1 atm at 300K, followed by 300 ns NPT production at 300 K. The first 60 ns of each MDS were discarded as equilibration time.

Anchor prediction

Hierarchical clustering (Kozakov, Clodfelter, Vajda & Camacho, 2005) determined the most stable conformation of dipeptides between A_1 and L_5. Clustering is based on the Root Mean Square Deviation (RMSD) between MDS snapshots less than 1 A for A_1R_2, R_2S_3, S_3R_4, and R_4L_5. We also determined the contacts of side chains as a proxy for ability to bind the receptor, i.e., if side chains are interacting with each other, their interaction with the receptor is hindered. Atomic contacts are defined as atoms from the peptide that are less than 3.8 A of Cβ-alanine, [Nε, NH2]-arginine, Cβ-serine, [Cδ1, Cδ2]-leucine from dipeptides. The prediction is that the stable motif accessible to solvent is critical for molecular recognition, i.e., the anchor of the protein-protein interaction (Rajamani, Thiel, Vajda & Camacho, 2004).

Virtual screening of ZINC database

We used the anchor motif as template to design and refine pharmacophore models to virtually screen more than 27 million compounds using the public server ZINCPharmer (Koes & Camacho, 2012). Based on A_1R_2 configuration we screened near to 27 million commercially available compounds using ZINCPharmer, resulting in the compounds studied here.

Synthesis of CBD3063

Step 1. 3-acetamidopiperidine-1-carbonyl chloride

In a cooled (0 °C) solution of *N* -(piperidin-3-yl)acetamide (500 mg, 3.52 mmol) in anhydrous dichloromethane (20 mL) was added $NaHCO_3$ (1.10 g, 10.6 mmol) and triphosgene (696 mg, 2.34 mmol). The mixture was stirred at room temperature for 1 hour. After all starting material has been consumed, the mixture was filtered, and the collected filtrate was evaporated under reduced pressure. The resulting residue was then allowed to passed through a short silica plug (wash with 100% EtOAc) to yield crude 3-acetamidopiperidine-1-carbonyl chloride (467 mg, 65%) as sticky transparent liquid (HRMS calcd for $C_8H_{14}ClN_2O_2^+$[M+H]$^+$: 205.0748; found: 205.0738). The compound was used immediately for the next step without further purification.

Step 2. 3-acetamido-*N* -(3-(pyridin-2-ylamino)propyl)piperidine-1-carboxamide

3-acetamidopiperidine-1-carbonyl chloride (100 mg, 0.489 mmol) from the previous step was dissolved in anhydrous dichloromethane (5.0 mL). Into this solution was added Na_2CO_3 (104 mg, 0.977 mmol) and*N* ^{1}-(pyridin-2-yl)propane-1,3-diamine (73.9 mg, 0.489 mmol). The mixture was stirred for 2 hours, upon which all starting material had reacted. The mixture was filtered, and the collected filtrate was evaporated under reduced pressure. The resulting residue was then purified by flash column chromatography (gradient elution of 0% to 10% MeOH in CH_2Cl_2) to yield**3-** acetamido-*N* -(3-(pyridin-2-ylamino)propyl)piperidine-1-carboxamide (137 mg, 88%) as white foam solid. ^{1}H NMR (600 MHz, $CDCl_3$) δ 7.99 (dd, J = 4.1, 0.8 Hz, 1H), 7.38 (ddd, J = 8.7, 7.1, 1.9 Hz, 1H), 6.53 (ddd, J = 7.0, 5.2, 0.8 Hz, 1H), 6.41 (d, J = 8.4 Hz, 1H), 6.12 (d, J = 6.5 Hz, 1H), 5.79 (t, J = 5.5 Hz, 1H), 5.10 – 4.95 (m, 1H), 3.99 – 3.86 (m, 1H), 3.45 – 3.36 (m, 6H), 3.32 (q, J = 6.1 Hz, 2H), 1.95 (s, 3H), 1.87 – 1.62 (m, 5H), 1.61 – 1.49 (m, 1H).^{13}C NMR (151 MHz, $CDCl_3$) δ 170.10, 158.60, 158.46, 147.02, 137.59, 112.50, 108.28, 48.66, 45.61, 44.60, 38.63, 37.69, 30.22, 29.40, 23.37, 22.23. HRMS calcd for $C_{16}H_{25}N_5O_2Na$ [M+Na]$^+$: 342.1900; found: 342.1908.

Culturing of CAD cell lines

Mouse neuron derived Cathecholamine A differentiated CAD cells (ECACC Cat# 08100805, RRID: CVCL_-0199) were grown in standard cell culture conditions, 37 °C in 5% (vol/vol) CO_2. The cells were maintained in DMEM/F12 media supplemented with 10% (vol/vol) FBS (HyClone) and 1% penicillin/streptomycin sulfate from 10,000 μg/mL stock.

Immunoprecipitation (IP) of endogenous CRMP2

CAD cells were incubated overnight with vehicle (0.1 % DMSO) or CBD3063 (20 μM). The next day the cells were lysed into the IP buffer containing 20 mM Tris-HCl pH=7.4, 50 mM NaCl, 2 mM $MgCl_2$, 10 mM N-Ethylmaleimide (NEM), 1% (vol/vol) NP-40, 0.5% (mass/vol) sodium deoxycholate, 0.1% (mass/vol) sodium dodecyl sulfate (SDS) with protease inhibitors (Cat# B14002, Biotool, Houston, TX), phosphatase inhibitors (Cat# B15002, Biotool, Houston, TX) and Nuclease (Cat# 88701, Thermo Fisher Scientific, Waltham, MA). Total protein concentration was determined by BCA protein assay kit (Cat# PI23225, Thermo Fisher Scientific, Waltham, MA). Five hundred micrograms of total protein were incubated overnight with 2 μg of CRMP2 antibody (Cat# C2993, Sigma-Aldrich, St. Louis, MO) at 4°C under gentle agitation. Protein G magnetic beads (Cat# 10004D, Thermo Fisher Scientific, Waltham, MA), pre-equilibrated with the immunoprecipitation buffer, were then added to the lysates and incubated for 2 h at 4°C to capture immuno-complexes. Beads were washed four times with IP buffer to remove nonspecific binding of proteins, before resuspension in Laemmli buffer and boiling at 95°C for 5 min prior to immunoblotting.

Immunoblot preparation and analysis

Indicated samples were loaded on 4–20% Novex gels (cat. no. XP04205BOX; Thermo Fisher Scientific, Waltham, MA). Proteins were transferred to preactivated PVDF membranes for 1 h at 100 V using TGS [25 mM Tris, pH 8.5, 192 mM glycine, 0.1% (mass/vol) SDS], 20% (vol/vol) methanol as transfer buffer (0.45 μm; Cat# IPVH00010; Millipore Sigma, St. Louis, MO). After transfer, the membranes were blocked at room temperature for 1 h with TBST (50 mM Tris·HCl, pH 7.4, 150 mM NaCl, 0.1% Tween 20) with 5% (mass/vol) nonfat dry milk, and then incubated overnight at 4 °C separately with indicated primary antibodies, βIII-Tubulin (Cat# G7121; Promega, Madison, WI), CRMP2 (Cat# C2993; Sigma-Aldrich, St.

Louis, MO), $Ca_v2.2$ (Cat# TA308673; Origene, Rockville, MD), CRMP2 pSer522 (Cat# CP2191; ECM Biosciences, Versailles, KY), CRMP2 pThr514 (Cat# PA5-110113; Invitrogen, Waltham, MA), in TBST, 5% (mass/vol) BSA. For examining the effect of CBD3063 on CRMP2 phosphorylation state, CAD cells were treated overnight with vehicle (0.1 % DMSO) or CBD3063 (20 μM) and the next day cells were lysed using RIPA buffer. Approximately 40 μg of total proteins were loaded on an SDS-PAGE and then transferred to polyvinylidene difluoride membranes and blocked at room temperature for 1 hour. Primary antibodies used for probing were CRMP2 (Cat# C2993, Sigma-Aldrich, St Louis, MO), CRMP2 pThr514 (Cat# PB-043, Kinasource, Dundee, Scotland, United Kingdom), CRMP2 pSer522 (Cat# CP2191, ECM Biosciences, Versailles, KY), and CRMP2 pT555 (Cat# CP2251, ECM Biosciences, Versailles, KY). Following incubation in HRP-conjugated secondary antibodies from Jackson Immuno Research (West Grove, PA), blots were revealed by enhanced luminescence (WBKLS0500; Millipore Sigma St. Louis, MO).

Animals

Pathogen-free adult male and female Sprague-Dawley rats (˜75-100 g, Charles River Laboratories, Wilmington, MA.) were kept in light (12-h light: 12-h dark cycle; lights on at 07:00 h) and temperature (23 ± 3°C) controlled rooms. Standard rodent chow and water were available *ad libitum.* All animal use was conducted in accordance with the National Institutes of Health guidelines, and the study was conducted in strict accordance with recommendations in the Guide for the Care and Use of Laboratory Animals of the New York University (Protocol#: PROTO202100104). All animals were housed and bred at the New York University Kriser Dental Center Animal Facility. All efforts were made to minimize animal suffering.

Dorsal root ganglion neuron cultures

Lumbar DRGs were dissected from 100 g female Sprague-Dawley rats using procedures as described previously (Gomez et al., 2022). DRGs were excised and placed in sterile DMEM (Cat# 11965; Thermo Fisher Scientific, Waltham, MA). The ganglia were dissociated enzymatically with collagenase type I (5 mg/mL, Cat# LS004194; Worthington) and neutral protease (3.125 mg/mL, Cat# LS02104; Worthington, Lakewood, NJ) for 50 minutes at 37°C under gentle agitation. The dissociated cells were then centrifuged (800 rpm for 5 min) and resuspended in DMEM containing 1% penicillin/streptomycin sulfate (Cat# 15140, Life Technologies, Carlsbad, CA), 10% fetal bovine serum [HyClone]) and 30 ng/mL nerve growth factor (Cat# N2513, Millipore Sigma, St. Louis, MO). The cells were seeded on poly-D-lysine (Cat# P6407, Millipore Sigma, St. Louis, MO) and laminin (Cat#sc-29012, Santa Cruz Biotechnology, Dallas, TX) -coated 12- or 15-mm glass coverslips and incubated at 37°C. All cultures were used within 48 hours.

Immunocytochemistry and confocal microscopy

Immunocytochemistry was performed on DRG neurons incubated with vehicle (0.1 % DMSO) or CBD3063 (20 μM) overnight. Cultured DRG neurons were fixed using ice-cold methanol for 5 min and then allowed to dry at room temperature. Fixed cells were rehydrated in PSB and then blocked with PBS containing 3% bovine serum albumin for 30 min at room temperature. Cell staining was performed with anti-$Ca_v2.2$ (Origene, Cat# TA308673, Rockville, MD) in PBS with 3% BSA overnight at 4°C. The cells were then washed thrice in PBS and incubated with PBS containing 3% BSA and secondary antibodies (Alexa 488 Chicken anti-Rabbit (Life Technologies, Carlsbad, CA)) for 1 h at room temperature. Coverslips were mounted and stored at 4°C until analysis. Immunofluorescent micrographs were acquired on a Leica SP8 inverted upright microscope using a 63X, oil immersion objective. For all quantitative comparisons among cells under differing experimental conditions, camera gain and other relevant settings were kept constant. The freeware image analysis program Image J (http://rsb.info.nih.gov/ij/) was used for quantifying cellular fluorescence. Regions of interest (i.e. cells) were defined by hand using Image J.

Calcium imaging

Changes in depolarization-induced calcium influx in rat DRG neurons were determined by loading neurons with 3 mM Fura-2AM for 30 minutes at 37°C (Cat# F1221; Thermo Fisher Scientific, Waltham, MA, stock solution prepared at 1 mM in DMSO, 0.02% pluronic acid, Cat# P-3000MP; Life Technologies, Carlsbad,

CA) as previously described (Bellampalli et al., 2019). DRG neurons were incubated overnight with 20 μM of test compounds. A standard bath solution containing 139 mM NaCl, 3 mM KCl, 0.8 mM $MgCl_2$, 1.8 mM $CaCl_2$, 10 mM Na-HEPES, 5 mM glucose, pH 7.4, was used. Depolarization was evoked with a 10 sec pulse of 90 mM KCl. Fluorescence imaging was achieved with an inverted microscope, Nikon Eclipse TE2000-U, using an objective Nikon Super Fluor 4X and a Photometrics-cooled CCD camera CoolSNAPHQ (Roper Scientific, Tucson, AZ) controlled by Nis Elements software (version 4.20; Nikon Instruments, Melville, NY). The excitation light was delivered by a Lambda-LS system (Sutter Instruments, Novato, CA). The excitation filters (340 ± 5 nm and 380 ± 7 nm) were controlled by a Lambda 10 to 2 optical filter change (Sutter Instruments, Novato, CA). Fluorescence was recorded through a 505-nm dichroic mirror at 535 ± 25 nm. Images were taken every ˜2.4 seconds during the time course of the experiment to minimize photobleaching and phototoxicity. To provide acceptable image quality, a minimal exposure time that provided acceptable image quality was used. Changes in $[Ca^{2+}]c$ were monitored following a ratio of F_{340}/F_{380}, calculated after subtracting the background from both channels.

Whole-cell patch-clamp recordings of Ca^{2+} and Na^{+} currents in acutely dissociated DRG neurons

Recordings were obtained from acutely dissociated DRG neurons as described earlier (Bellampalli et al., 2019). Patch-clamp recordings were performed at room temperature (22–24°C). Currents were recorded using an EPC 10 Amplifier-HEKA (HEKA Elektronik, Ludwigshafen, Germany) linked to a computer with Patchmaster software. DRG neurons were incubated overnight (˜16-24 h) with 20 μM of CBD3063.

For total calcium current (ICa^{2+}) recordings, the external solution consisted of the following (in mM): 110 N-methyl-D-glucamine, 10 $BaCl_2$, 30 TEA-Cl, 10 HEPES, 10 glucose, 0.001 TTX (pH 7.29 adjusted with TEA-OH, and mOsm/L= 310). Patch pipettes were filled with an internal solution containing (in mM): 150 $CsCl_2$, 10 HEPES, 5 Mg-ATP, and 5 BAPTA, (pH 7.2 adjusted with CsOH, and mOsm/L= 305). Peak Ca^{2+2+}channels, DRGs were treated with a Ca_v inhibitor cocktail omitting the inhibitor specific to the subtype being tested (e.g., to measure $Ca_v2.2$ currents, ω-conotoxin GVIA is omitted): Nifedipine (10 μM, L-type), ω-Conotoxin-GVIA (500 nM, P/Q-type) (Feng, Hamid, Doering, Bosey, Snutch & Zamponi, 2001), SNX482 (200 nM, R-type) (Newcomb et al., 1998), ω-agatoxin (200 nM, P/Q-type) (Mintz, Venema, Swiderek, Lee, Bean & Adams, 1992), TTA-P2 (1 μM, T-type) (Choe et al., 2011).

For Na^{+} current (I_{Na+}) recordings, the external solution contained (in mM): 130 NaCl, 3 KCl, 30 tetraethylammonium chloride, 1 $CaCl_2$, 0.5 $CdCl_2$, 1 $MgCl_2$, 10 D-glucose and 10 HEPES (pH 7.3 adjusted with NaOH, and mOsm/L= 324). Patch pipettes were filled with an internal solution containing (in mM): 140 CsF, 1.1Cs-EGTA, 10 NaCl, and 15 HEPES (pH 7.3 adjusted with CsOH, and mOsm/L= 311). Peak Na^{+}

To isolate potassium currents (I_{K+}), DRG neurons were bathed in external solution composed of (in millimolar): 140 N-methyl-glucamine chloride, 5 KCl, 1 $MgCl_2$, 2 $CaCl_2$, 10 D-glucose and 10 HEPES (pH adjusted to 7.3 with KOH and mOsm/L= 313). Recording pipettes were filled with internal solution containing (in mM): 140 KCl, 2.5 $MgCl_2$

Normalization of currents to each cell's capacitance (pF) was performed to allow for collection of current density data. For I-V curves, functions were fitted to data using a non-linear least squares analysis. I-V curves were fitted using double Boltzmann functions:

$f = a + g1/(1+exp((x-V_{1/2}1)/k1)) + g2/(1+exp(-(x-V_{1/2}2)/k2))$

where x is the pre-pulse potential, $V_{1/2}$is the mid-point potential and k is the corresponding slope factor for single Boltzmann functions. Double Boltzmann fits were used to describe the shape of the curve, not to imply the existence of separate channel populations. Numbers *1* and *2* simply indicate first and second mid-points; a along with g are fitting parameters.

Activation curves were obtained from the I-V curves by dividing the peak current at each depolarizing step by the driving force according to the equation: $G= I/(V_{mem}- E_{rev})$, where I is the peak current, V_{mem} is the membrane potential and E_{rev} is the reversal potential. The conductance (G) was normalized against the

maximum conductance (G_{max}). For total and the different subtypes of Ca^{2+}For $Na^{+}{}_{max}$). Activation and SSI curves were fitted with the Boltzmann equation.

Indwelling intrathecal catheter

Rats were anesthetized with ketamine/xylazine 80/12 mg/kg intraperitoneally (i.p.) (Sigma-Aldrich, St. Louis, MO), and their head was placed in a stereotaxic frame. The cisterna magna was exposed and incised. As previously reported, an 8-cm catheter (PE-10; Stoelting, Wood Dale, IL) was implanted, terminating in the lumbar region of the spinal cord (Yaksh & Rudy, 1976). Catheters were sutured (using 3–0 silk sutures) into the deep muscle and externalized at the back of the neck. Autoclips were used to close the skin, and other surgeries were performed after a 5- to 7-day recovery period.

Spared nerve injury (SNI) model of neuropathic pain

The neuropathic pain model induced by spared nerve injury (SNI) in rats was performed as previously described. Adult male rats (250 g, Envigo, Placentia, CA) were anesthetized with isoflurane (5% induction, 2% maintenance in 2 L/min air), and skin on the lateral surface of the left hind thigh was incised. Then, the biceps femoris muscle was dissected to expose the three terminal branches of the sciatic nerve. The common peroneal and tibial branches were tightly ligated with 4-0 silk and axotomized 2.0 mm distal to the ligation. Closure of the incision was made in two layers. The muscle was sutured once with 5-0 absorbable suture; skin was autoclipped. Animals were allowed to recover for 7 days before any testing. On the 7^{th} day after SNI, CBD3063 (0.3 μg/kg) or 1% DMSO was injected intrathecally. Mechanical allodynia was assessed 10 days after surgery.

Measurement of mechanical allodynia

Mechanical allodynia was assessed by measuring rats' paw withdrawal threshold in response to probing with a series of fine calibrated filaments (von Frey, Stoelting, Wood Dale, IL). Rats were placed in suspended plastic cages with wire mesh floor, and each von Frey filament was applied perpendicularly to the plantar surface of the paw. The "up-and-down" method (sequential increase and decrease of the stimulus strength) was used to determine the withdrawal threshold Dixon's nonparametric method was used for data analysis, as described by Chaplan et al (Chaplan, Bach, Pogrel, Chung & Yaksh, 1994). Data were expressed as the mean withdrawal threshold.

Data Analysis

Graphing and statistical analysis was performed with GraphPad Prism (Version 9). All data sets were checked for normality using D'Agostino & Pearson test. Details of statistical tests, significance and sample sizes are reported in the appropriate figure legends. All data plotted represent mean ± SEM. For western blot experiments, statistical differences between groups were determined by unpaired t test or Mann-Whitney test. Statistical significance of confocal imaging data was evaluated by Mann-Whitney test. For electrophysiological recordings: Normalized peak currents were analyzed by Kruskal-Wallis test followed by the Dunn's post hoc test; the significance of the I-V curves was analyzed by multiple Mann-Whitney tests; peak current density as well as $V_{1/2}$ midpoint potential and k slope factor were compared using Mann-Whitney test. For resting membrane potential and rheobase, the significance was analyzed by Mann-Whitney test; the significance of the number of evoked action potentials per step was analyzed by multiple Mann-Whitney tests. Behavioral data was analyzed by multiple Mann-Whitney tests and Mann-Whitney test for time-course experiments and area under the curve respectively. Detailed statistical analyses are presented in **Table S1** .

Nomenclature of Targets and Ligands

Key protein targets and ligands in this article are hyperlinked to corresponding entries in http://www.guidetopharmacology.org, and are permanently archived in the Concise Guide to PHARMACOLOGY 2021/22 (Alexander et al., 2021).

Results

Stability analysis of CBD3 peptide predicts A_1R_2 dipeptide as a suitable target for small molecule peptidomimetics

Underlying molecular recognition is the ability of a ligand to present a suitable structural motif for at least a few nanoseconds to efficiently engage its receptor (Rajamani, Thiel, Vajda & Camacho, 2004). In the far-western assay using 15-mer peptides (overlapping by 12 amino acids) of full-length CRMP2 revealed that the highest binding to $Ca_v2.2$ was attained by peptide *ARSRLAELRGVPRGL*(CBD3) (Brittain et al., 2011b). Subsequent work showed that the first six amino acids *ARSRLA* were critical for binding, mutagenesis suggested that two residues (Ala_1 and Arg_4) were important for binding (Moutal et al., 2018). To predict the recognition motif in CBD3, we performed three independent molecular dynamics simulations (MDS) of the full peptide and of the TAT conjugated peptide and scanned the trajectories for the most stable dipeptide conformation (**Figure 1A; see also Figure S1**), as well as assessed whether the corresponding side chains are blocked by intra-peptide contacts or are exposed to solvent and free to interact (**Figure 1B**). Simulations showed that A_1R_2 dipeptide, formed the most stable solvent exposed motif, while the rest of the peptide was mostly cluttered (**Figure 1A, B**).

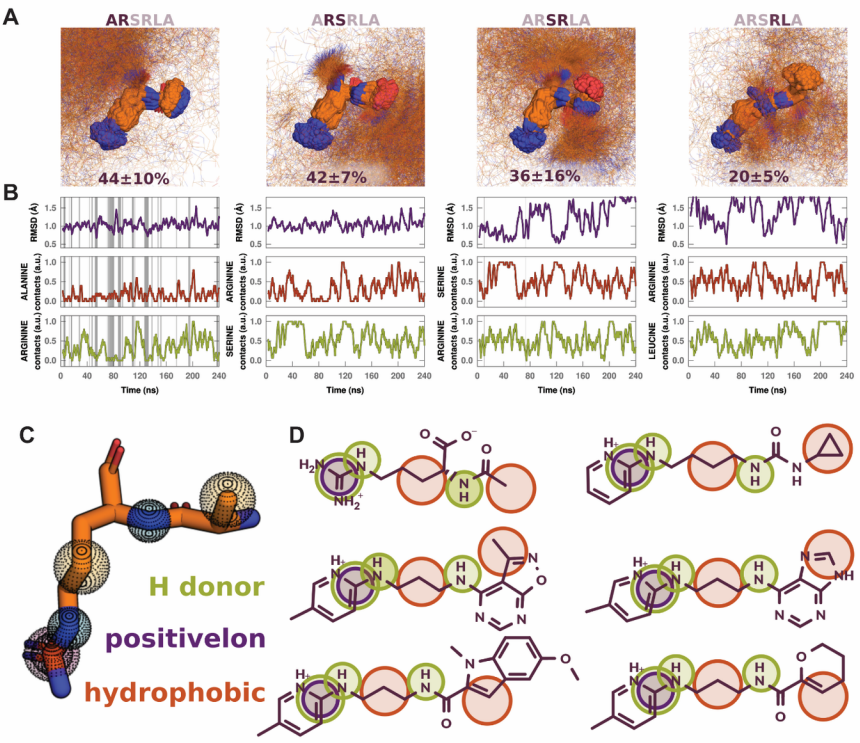

Figure 1. Stability analysis of dipeptides within CBD3 and pharmacophore model on average cluster center of A_1R_2 dipeptide and sample of matched hits. (A) Largest cluster of MD snapshots with RMSD less than 1 Å for dipeptides A_1R_2, R_2S_3, S_3R_4 *and* R_4L_5 , also shown is average percentage of cluster size in 3 independent simulations. (B) RMSD relative to cluster center and times the amino acid side chains are free of contacts (3.8 Å for hydrogen bond donors and 4 Å for hydrophobic side chains) within 3 ns windows in a representative MD trajectory of CBD3 peptide. Gray regions highlight regions for which RMSD of snapshots are less than 1 Å from cluster center, and side chains are 80% or more free of contacts within 3 ns windows. (C) Pharmacophores radiuses used: guanidine group, 0.78 Å for positive ion and 1 Å for hydrogen bond donor; 0.78 Å for other hydrogen bond donors, and 1.0 Å for hydrophobic atoms. (D) Sample of compounds that matched all pharmacophores using ZincPharmer.

TheA_1R_2 structural motif shown in**Figure 1A** , defined as the conformation having the largest 1 Å radius cluster of snapshots in our MDS, encompassed about 44% of our total runs. Furthermore, since previously reported cell-based experiments also involved the cell-penetrating tat sequence conjugated to CRMP2 derived peptides, we repeated the MDS on the full tat-*ARSRLA* sequence, obtaining the same structural motif as for CBD3 (**Figure S1**). The robustness of theA_1R_2 motif led us to use it as the basis for the design of the pharmacophore model shown in**Figure 1C** . We entered this design in the open access server ZincPharmer (*http://zincpharmer.csb.pitt.edu/*) to search for suitable compounds among more than 27 million commercially available compounds from the ZINC database (Sterling & Irwin, 2015), obtaining ˜200 hits. Based on availability and manual curation, we selected 77 compounds for experimental validation (**Figure 1D**). **Figure S2** shows the full list of compounds.

Compound screening in sensory neurons

We previously reported that targeting the $Ca_v2.2$–CRMP2 interaction with tat-CBD3 (Brittain et al., 2011b) or myr-tat-CBD3 (Francois-Moutal et al., 2015) peptides results in reduction of depolarization-induced Ca^{2+}-influx in sensory neurons. Here, we used this approach for experimental validation. For this, we used Fura 2-AM-based ratiometric Ca^{2+}-imaging in rat DRG neurons. To activate high-voltage-activated (HVA) Ca^{2+} channels, we challenged DRG neurons from all sizes with 90 mM KCl (Gomez et al., 2022). We have previously demonstrated that acute application (5-30 minutes) of 20 μM of myr-tat-CBD3 peptide was unable to inhibit Ca^{2+}influx. In contrast, chronic application (˜24 hours) of 20 μM of myr-tat-CBD3 peptide inhibited Ca^{2+} currents by ˜40% (Francois-Moutal et al., 2015). Hence, overnight incubation of 20 μM of test compounds was utilized to assess the activity of these compounds.

Our *in vitro* screening showed that stimulation of DRG neurons with 90 mM KCl led to an increase in Ca^{2+} influx as shown in the control group (0.05% DMSO; **Figure 2A**). Overnight incubation with 20 μM of the test compounds revealed that, of the 77 compounds tested, nine of them (CBD3018, 3026, 3033, 3038, 3039, 3062, 3063, 3065 and 3074) inhibited Ca^{2+} influx by more than 50% relative to the DMSO-treated (i.e., control) group (**Figure 2A**). With one exception (CBD3026), all identified antagonists contained similar chemotypes – a protonated moiety and two dimethylamines, as well as the alanine hydrophobic moiety (**Figure S3**). Indeed, all nine compounds can be assigned to only two chemical classes and three chemotypes. Specifically, CBD3018, 3026, 3062, 3065, 3074 belong to guanidines, CDB 3033, 3038, 3039 feature 2-aminopyridylpropylcarboxamide class, and CBD3062 and 3063 are of analogous 2-aminopyridylpropylurea chemotype. Overall, these results show that these first-in-class compounds predicted to disrupt $Ca_v2.2$–CRMP2 interaction decrease HVA channel activity in DRG neurons from all sizes and share chemically similar motifs.

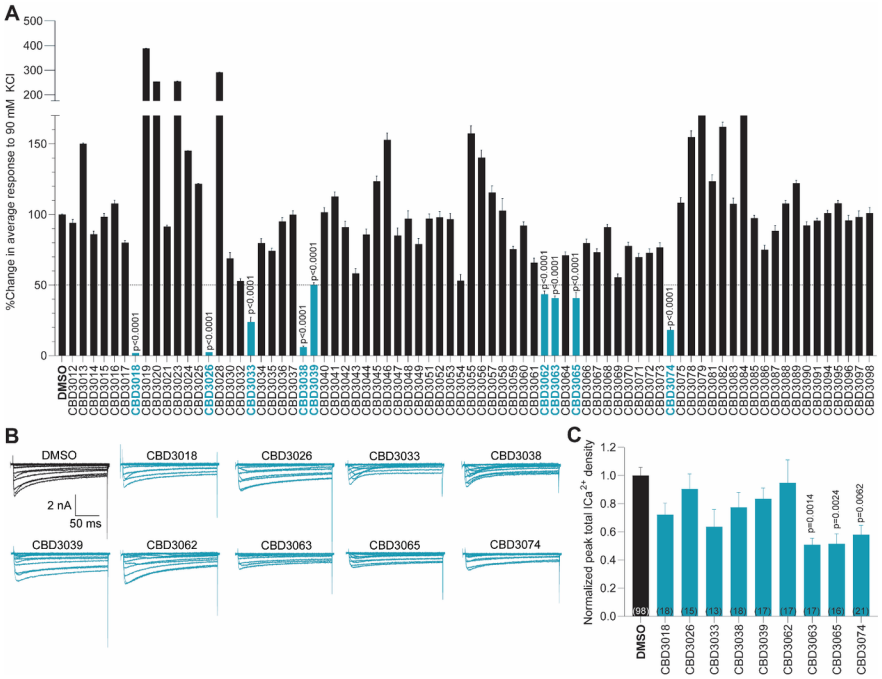

Figure 2. Compound screening using depolarization-induced Ca^{2+} influx and whole-cell patch-clamp in DRG neurons identify various high-voltage-activated Ca^{2+} channels inhibitors. (A) Percent change in average response of DRG sensory neurons incubated overnight with 20 μM of the indicated compounds in response to 90 mM KCl. N=61-629 cells; error bars indicate mean ± SEM.p values as indicated; One-Way ANOVA with the Dunnett post hoc test. Only the significances for the compounds that inhibit Ca^{2+2+} density. N=16-98 cells indicated in parenthesis; error bars indicate mean ± SEM; p values as indicated; Kruskal-Wallis test followed by Dunn's post hoc test.

CBD3 compounds inhibit total Ca^{2+} currents in sensory neurons

The calcium imaging results do not discriminate between small, medium and large diameter DRG neurons, therefore we next dissected the effects of the top compounds on a subpopulation of small-to-medium diameter nociceptive neurons (Basbaum, Bautista, Scherrer & Julius, 2009) since large-diameter DRG neurons in normal conditions transduce mechanical and proprioceptive information. The medium and small DRG neurons belong to lightly myelinated Aδ and unmyelinated C fibers, respectively. These primary afferent fibers are necessary for pain transmission since they send nociceptive information to the dorsal horn of the spinal cord (Basbaum, Bautista, Scherrer & Julius, 2009); thus, we performed whole-cell patch-clamp recordings in small-to-medium diameter DRG neurons from female rats to electrophysiologically validate the nine top compounds that blocked Ca^{2+} influx.

DRGs were treated overnight with 20 μM of test compounds or vehicle (0.1% DMSO). Inward current through Ca^{2+} channels was carried by Ba^{2+} and will be referred to it as Ca^{2+} currents. From a holding potential of -90 mV, 200-ms depolarization steps from -70 to +60 mV in 10 mV increments, we elicited a family of Ca^{2+} currents (**Figure 2B**). We next obtained the peak current density and normalized it to the control group (**Figure 2C**) and found that CBD3063, 3065 and 3074 significantly reduced total Ca^{2+} currents when compared to cells treated with 0.1% DMSO (DMSO: 1.00 ± 0.06 pA/pF; CBD3063: 0.51 ± 0.04 pA/pF; CBD3065: 0.52 ± 0.07 pA/pF; CBD3074: 0.58 ± 0.06 pA/pF).

Of the three compounds that inhibited Ca^{2+} currents, CBD3063 and CBD3065 represent unique chemotypes (**Table 1**) and were selected for additional characterization. However, in preliminary tests, CBD3065 did not exhibit analgesic properties (data not shown). Thus, CBD3065 was not further pursued. We measured current

density–voltage relationships and observed that incubation with 20 μM of CBD3063 significantly decreased Ca^{2+} current density from 0 to 30 mV (**Figure 3A, B**). Furthermore, at peak current density (+10 mV; **Figure 3C**), the reduction in Ca^{2+} currents imposed by CBD3063 was ˜46.54% when compared to cells treated with 0.1% DMSO (DMSO: -93.23 ± 10.40 pA/pF; CBD3063: -49.84 ± 6.17 pA/pF). Inspection of voltage–dependence of activation revealed no difference in the half activation potential and slope factors between groups (**Figure 3D** and **Table 2**). We also assessed steady–state inactivation kinetics of the channels at multiple test potentials by measuring the fraction of current remaining at +10 mV. As seen in **Figure 3D**and **Table 2** , our results revealed no significant differences in half inactivation potential and slope factors between the conditions. Collectively, our findings indicate that our top compound – CBD3063 – inhibits Ca^{2+} currents in small-to-medium diameter (i.e., presumptively nociceptive) sensory neurons.

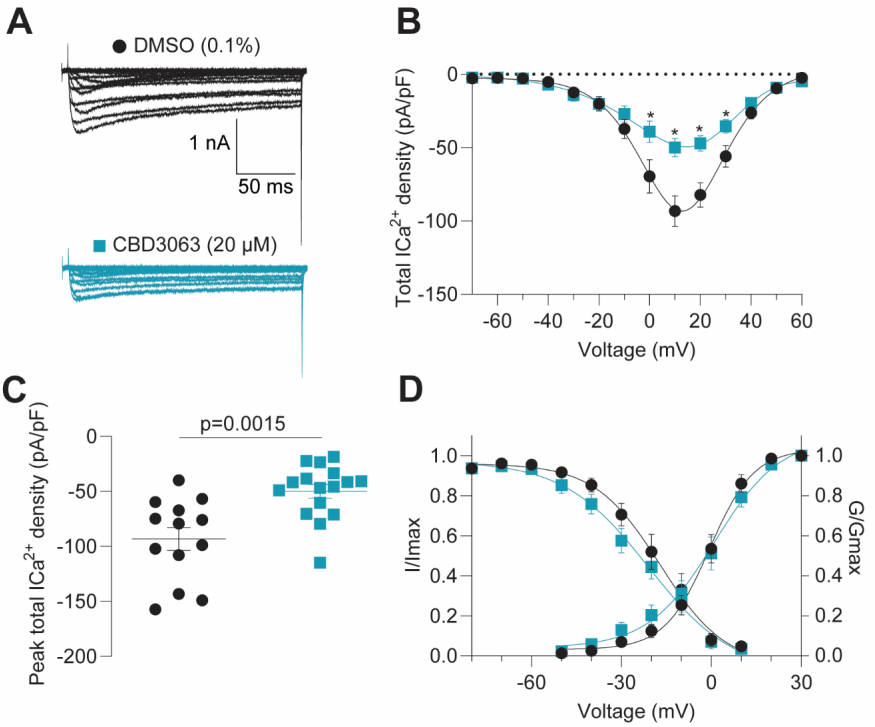

Figure 3. CBD3063 reduces total calcium currents in DRG neurons. p <0.05; Multiple Mann-Whitney tests. (C) Summary of bar graph showing peak calcium current densities (pA/pF).p value as indicated; Mann-Whitney test. (D) Boltzmann fits for voltage-dependent activation and inactivation as shown. Half-maximal activation potential of activation and inactivation ($V_{1/2}$) and slope values (k) for activation and inactivation are presented in **Table 2** . N=13-16 cells; error bars indicate mean ± SEM.

CBD3063 disrupts $Ca_v2.2$–CRMP2 binding and impairs membrane trafficking of $Ca_v2.2$ channels without effecting CRMP2 phosphorylation

We previously reported that tat-CBD3 (Brittain et al., 2011b) and myr-tat-CBD3 (Francois-Moutal et al., 2015) peptides inhibit the $Ca_v2.2$–CRMP2 interaction and reduced surface expression of $Ca_v2.2$. Therefore, we next asked if CBD3 peptidomimetic CBD3063 could interfere with $Ca_v2.2$–CRMP2 binding and affect the membrane localization of $Ca_v2.2$ channels. For this, catecholamine A differentiated (CAD) cells – a mouse neuronal cell line expressing both CRMP2 and $Ca_v2.2$ – were incubated overnight with 0.1% DMSO or 20 μM CBD3063. Immunoprecipitation assays revealed an ˜35% reduction in the level of $Ca_v2.2$ protein immunoprecipitated by CRMP2 in cells treated with CBD3063 versus control (**Figure 4A, B** ; DMSO: 1.00 ± 0.05; CBD3063: 0.64 ± 0.02). These results provide evidence that CBD3063 inhibits the association

between $Ca_v2.2$ and CRMP2.

We reported previously that CRMP2 facilitates the trafficking of $Ca_v2.2$ to the plasma membrane (Brittain, Piekarz, Wang, Kondo, Cummins & Khanna, 2009; Chi et al., 2009) and that cell-penetrant CBD3 peptides (Brittain et al., 2011b; Francois-Moutal et al., 2015; Xie et al., 2016) decrease surface trafficking of $Ca_v2.2$. Having established that CBD3063 can inhibit $Ca_v2.2$–CRMP2 interaction *in vitro* , we next asked if CBD3063 alters the subcellular localization of $Ca_v2.2$ channels. To evaluate this, DRG neurons were incubated with vehicle (0.1% DMSO) or CBD3063 (20 μM) overnight and subjected to immunofluorescent microscopy to assess the membrane expression of these channels. In control DRGs treated with vehicle, the fluorescent signal for $Ca_v2.2$ presents as an annulus at the plasma membrane (**Figure 4C**). As illustrated in **Figure 4D** , $Ca_v2.2$ expression in the membrane was significantly decreased when cells were incubated with CBD3063 (DMSO: 3.59 ± 0.42; CBD3063: 1.64 ± 0.10). These data suggests that by uncoupling $Ca_v2.2$–CRMP2 interaction, CBD3063 reduces surface trafficking of $Ca_v2.2$ channels to the plasma membrane of sensory neurons.

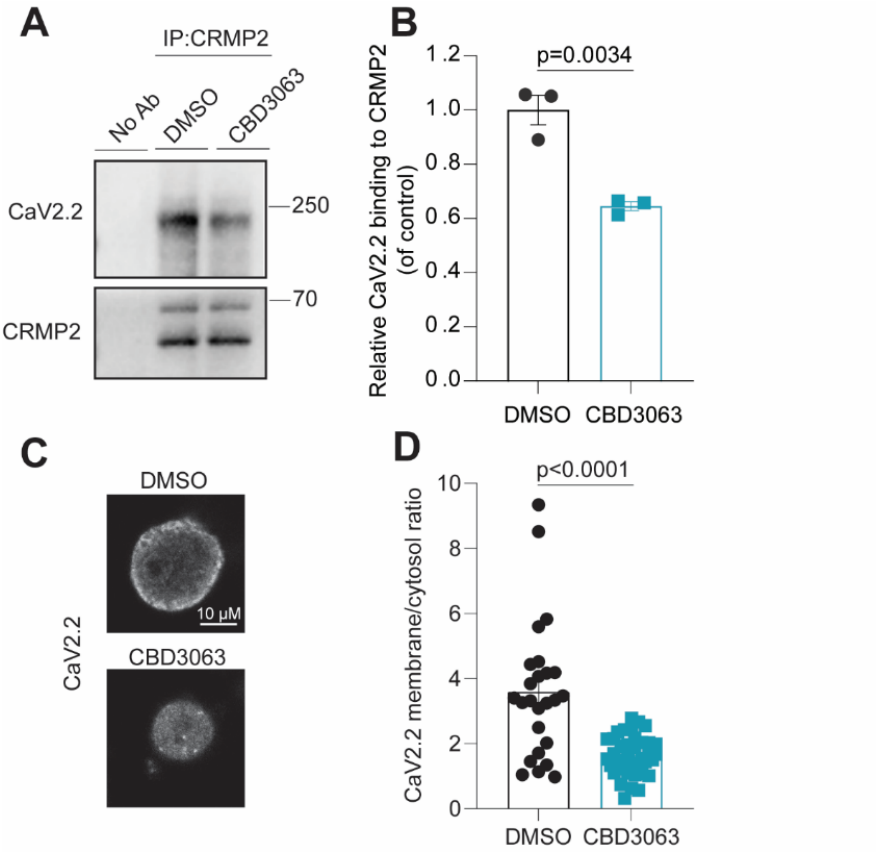

Figure 4. CBD3063 suppresses Ca $_v$2.2 –CRMP2 interaction and surface trafficking of the channel. Representative immunoblots (A) and summary (B) of CRMP2 immunoprecipitation (IP) to detect $Ca_v2.2$ from CAD cells treated overnight with CBD3063 (20 μM) (n=3). *p*value as indicated; Unpaired t-test. Representative micrographs of DRG cells immunolabeled with $Ca_v2.2$ (C) and summary (D) of $Ca_v2.2$ membrane/cytosol ratio in DRG neurons treated overnight with 20 μM of CBD3063 (n=25-38). Error bars show mean ± SEM;*p* values as indicated; Mann-Whitney test.

Because the cellular functions of CRMP2 are mediated by its phosphorylation, we next determined whether

CBD3063 could alter the phosphorylation states of CRMP2. Immunoblot analyses of lysates prepared from CAD cells exposed to overnight incubation of CBD3063 (20 μM) showed no differences in the expression of phosphorylated CRMP2 at sites 522 (by cyclin dependent kinase 5 (Cdk5); **Figure S4A, B**), 514 (by glycogen synthase kinase-3 beta (GSK-3β); **Figure S4C, D**), or 555 (RhoK; **Figure S4E, F**). These results rule out a potential side effect of CBD3063 on the phosphorylation status CRMP2.

CBD3063 selectively decreases $Ca_v2.2$ (N-type) Ca^{2+} currents in sensory neurons

We next asked if the CBD3063-mediated decrease in Ca^{2+}currents was due to our target $Ca_v2.2$ (N-type) channels. To test the minimum concentration needed to inhibit N-type Ca^{2+} channels' function, small-to-medium sized DRG neurons were treated overnight with 2, 20 and 50 μM of CBD3063 or control (0.1% DMSO). The next day, whole-cell patch-clamp recordings were performed in the presence of a cocktail of blockers of all other subtypes of calcium channels present in DRG neurons, thus isolating the N-type currents. When compared to DMSO-treated cells, 2 μM of CBD3063 did not modify the activity of these channels. On the contrary, 20 and 50 μM of CBD3063 significantly reduced peak current density, thus, 20 μM was sufficient to decrease N-type currents and used for further experimentation (DMSO: 1.00 ± 0.07; 2 μM CBD3063: 0.93 ± 1.07; 20 μM CBD3063: 0.74 ± 0.04; 50 μM CBD3063: 0.65 ± 0.06; **Figure 5A**). A significant decrease in N-type currents (**Figure 5B**) and current density at 0 and +10 mV (**Figure 5C**) was observed in cells incubated with 20 μM of CBD3063. At peak current density (+10 mV;**Figure 5D**), CBD3063 decreased N-type currents by ˜33.5% when compared to the control group (DMSO: -104.00 ± 11.32 pA/pF; CBD3063: -69.18 ± 6.54 pA/pF). Plotting voltage–dependence of activation and steady–state inactivation curves revealed no differences in half activation or inactivation potentials and slope factors between these two conditions (**Figure 5E** and**Table 2**). These data confirm that targeting the CRMP2–$Ca_v2.2$ interaction with CBD3063 decreases current influx through N-type Ca^{2+} channels.

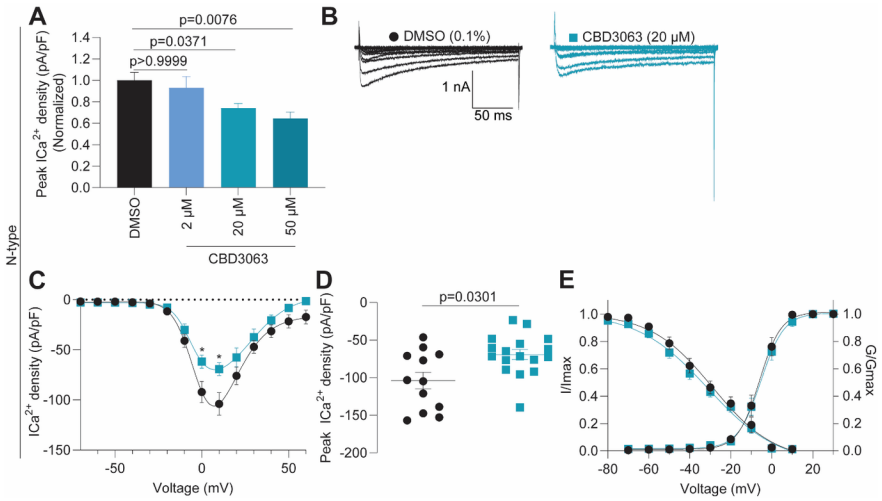

Figure 5. N-type ($Ca_v2.2$) calcium currents are reduced by CBD3063 in DRG neurons . (A) Summary of bar graph showing the normalized peak ICa^{2+} density after incubating sensory neurons with DMSO (0.1%), 2, 20 and 50 μM of CBD3063. N=13-30 cells; error bars indicate mean ± SEM; *pp* value as indicated; Mann-Whitney test. (E) Boltzmann fits for voltage-dependent activation and inactivation kinetics as shown. Half-maximal activation potential of activation and inactivation ($V_{1/2}$) and slope values (k) for activation and inactivation are presented in**Table 2** . N=12-17 cells.

Furthermore, to test any off-target effects of CBD3063 we measured current density–voltage curves and peak current densities for Ca_v1 (L-type; **Figure 6A, B**), $Ca_v2.1$ (P/Q-type; **Figure 6C, D**), $Ca_v2.3$ (R-type; **Figure 6E, F**), and Ca_v3 (T-type; **Figure 6G, H**) calcium channels. We found that CBD3063 does not alter Ca^{2+} influx through these channels when compared to cells treated with 0.1% DMSO. When the

voltage-dependence of activation and inactivation of these channels was explored, we observed that CBD3063 did not alter these parameters (**Table 2**). These findings show that CBD3063 selectively modulates the activity of N-type Ca^{2+}channels.

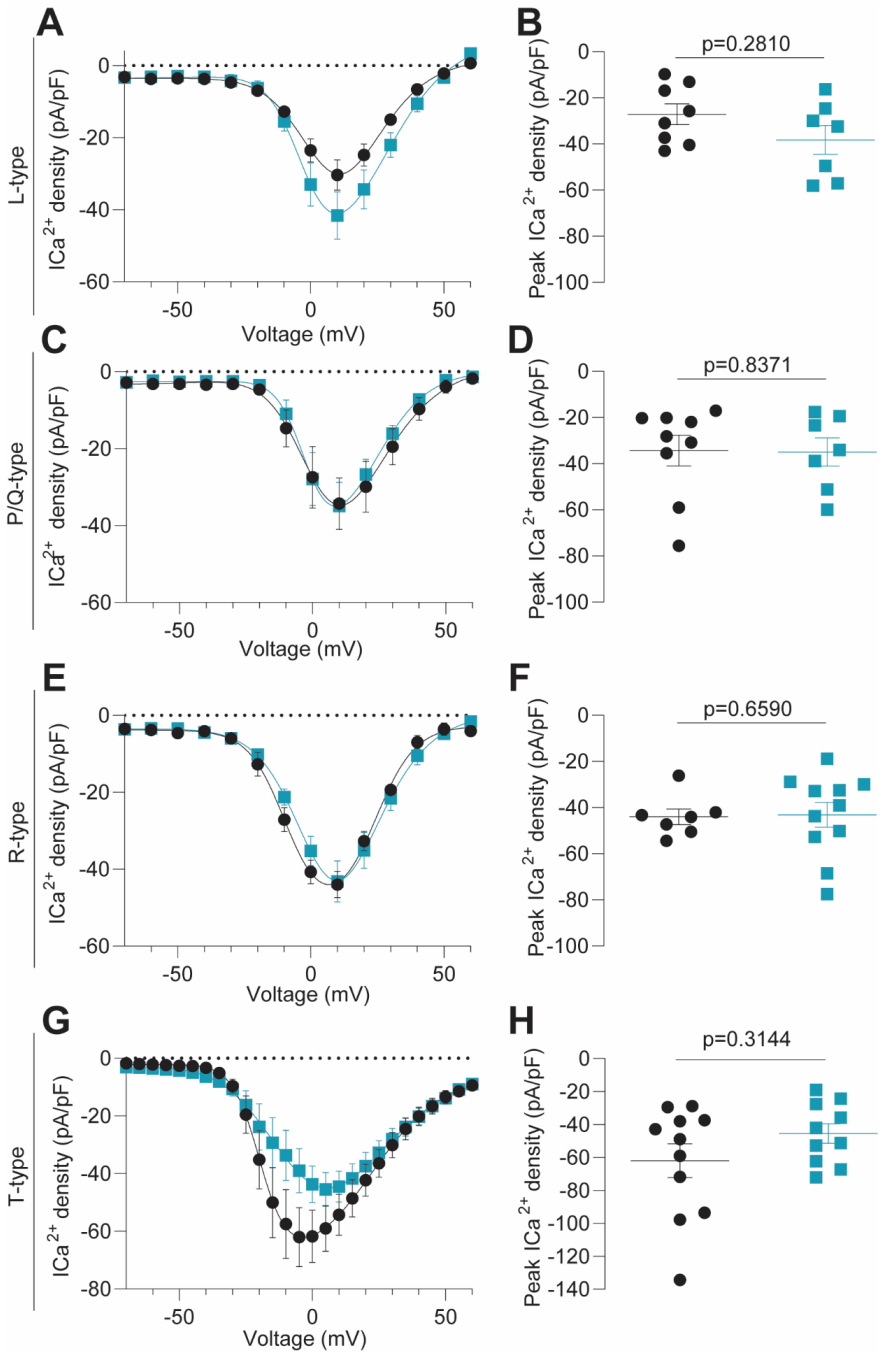

Figure 6. CBD3063 does not inhibit other voltage-gated calcium channels . (A, C, E, G) Double Boltzmann fits for L-, P/Q-. R-, and T-type current density–voltage curves respectively. Multiple Mann-Whitney tests. (B, D, F, H) Summary of bar graph showing peak L-, P/Q-. R-, and T-type calcium current densities (pA/pF). p value as indicated; Mann-Whitney test. N=7-11 cells; Error bars indicate mean ±

SEM; Half-maximal activation potential ($V_{1/2}$) and slope values (k) for activation and inactivation are presented in **Table 2** .

As CRMP2 has been reported to regulate the functional activity of Na^+ channels (Dustrude, Moutal, Yang, Wang, Khanna & Khanna, 2016; Dustrude, Perez-Miller, Francois-Moutal, Moutal, Khanna & Khanna, 2017; Dustrude, Wilson, Ju, Xiao & Khanna, 2013), we additionally tested if CBD3063 could affect Na^+currents in sensory neurons. CDB3063 did not affect Na^+ current density (DMSO: -455.7 ± 78.70 pA/pF; CBD3063: -455.0 ± 60.79 pA/pF) or gating properties of Na^+ channels in DRG neurons (**Figure S5** and**Table 2**). Furthermore, we found that CBD3063 had no effect on voltage-gated potassium channels (DMSO: 420.9 ± 54.19 pA/pF; CBD3063: 422.1 ± 52.70 pA/pF; **Figure S6**). Altogether, the above results demonstrate that CBD3063 specifically inhibits $Ca_V2.2$, sparing all other voltage-gated ion channels expressed in DRG sensory neurons.

CBD3063 decreases excitability of rat sensory neurons

$Ca_v2.2$ channels have critical roles in controlling the excitability of DRG neurons, according to earlier studies (Yang et al., 2018). Since $Ca_v2.2$ populations are affected by CBD3063, we next investigated whether CBD3063 may alter the excitability of DRG sensory neurons (**Figure 7**). Action potentials (AP) were elicited in rat sensory neurons during whole cell current-clamp tests in response to current injections from 0-120 pA after overnight incubation with 0.1% DMSO or 20 μM CBD3063. Representative traces are shown in**Figure 7A.** While the resting membrane potential remained unchanged between these two conditions (DMSO: -44.50 ± 1.478 mV; CBD3063: -50.00 ± 1.915 mV; **Figure 7B**), CBD3063 significantly increased the rheobase – the minimum current necessary to evoke an AP – compared to the control (DMSO: 15.00 ± 3.416 mV; CBD3063: 48.33 ± 9.098 mV; **Figure 7C**). CBD3063 also reduced the number of evoked APs over current injection steps ranging from 10 to 120 pA (**Figure 7D)** . These results show that CBD3063 mediated inhibition of the $Ca_v2.2$ channels culminates to curb sensory neuron excitability.

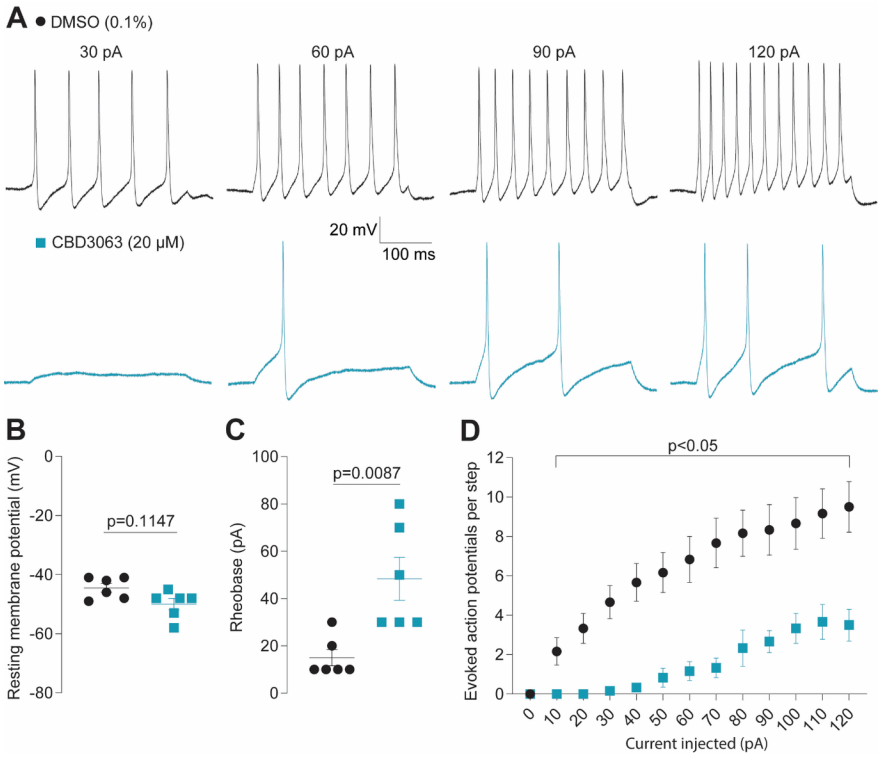

Figure 7. Sensory neuron excitability is decreased by CBD3063.(A) Representative traces in

response to the indicated current injection steps from rat DRG neurons treated 0.1% DMSO (control; black circles) or 20 μM CBD3063 (cyan squares). (B) Quantification of resting membrane potential in millivolts (mV) in the two conditions. (C) Quantification of the rheobase in the presence of DMSO or 20 μM CBD3063. (D) Summary of the number of evoked action potentials in response to current injection between 0-120 pA. N=6 cells; p value as indicated; Mann-Whitney test (B and C) and Multiple Mann-Whitney test. Error bars indicate mean ± SEM.

Disruption of $Ca_v2.2$ –CRMP2 binding confers antinociception

In humans, targeting auxiliary subunits that regulate $Ca_v2.2$ channels is effective against chronic pain. For example, targeting α2δ-1 subunit with Gabapentin and Pregabalin alleviates pain by interfering with $Ca_v2.2$–α2δ-1 interaction (Bauer, Rahman, Tran-van-Minh, Lujan, Dickenson & Dolphin, 2010; Hendrich et al., 2008; Sutton, Martin, Pinnock, Lee & Scott, 2002). Consequently, we tested if interrupting CRMP2 binding to $Ca_v2.2$ with CBD3063 could be antinociceptive in a rat model of spared nerve injury (SNI). This model of neuropathic pain results in long-lasting thermal hyperalgesia and mechanical allodynia on the affected hind paw (Decosterd & Woolf, 2000). We used male rats for these studies since interrupting the $Ca_v2.2$–CRMP2 interaction *in vivo* does not display sex dimorphism with equivalent effects observed in females (Ju, Li, Allette, Ripsch, White & Khanna, 2013; Ripsch, Ballard, Khanna, Hurley, White & Khanna, 2012) and males (Fischer, Pan, Vilceanu, Hogan & Yu, 2014; Francois-Moutal et al., 2015; Moutal et al., 2018).

Ligation of the tibial and peroneal nerves in male rats resulted in the development of mechanical hypersensitivity (**Figure 8**). We chose to administer CBD3063 intrathecally (0.3 μg/kg) to directly reach the site of action of $Ca_v2.2$ in the SDH, where the central termini of primary afferent fibers synapse with second order neurons in the SDH. A single intrathecal administration of CBD3063, 7 days following SNI, resulted in a significant reversal of mechanical allodynia that started 60 minutes post-injection and lasted up to 36 hours (**Figure 8A**). A significant increase in the area under the curve was observed after injection of CBD3063 compared to the control group (DMSO: 7.650 ± 0.84; CBD3063: 57.05 ± 3.84; **Figure 8B**).

To assess the long-term antinociceptive effect of CBD3063, rats were injected with CBD3063 (0.3 μg/kg) starting 7 days after SNI surgery and once a day for 14 days. On days 1, 3, 5, 7, 10 and 14, paw withdrawal thresholds were determined at six hours following each injection (**Figure 8C**). Repeated administration of CBD3063 resulted in a prolonged reversal of SNI-induced mechanical allodynia (**Figure 8C**). A significant increase in the area under the curve was observed following treatment with CBD3063 for 14 days (DMSO: 3.37 ± 0.86; CBD3063: 47.26 ± 8.22; **Figure 8D**). These results demonstrate that targeting the $Ca_v2.2$–CRMP2 interaction results in a long-lasting reversal of mechanical hypersensitivity, without any tolerance (loss of antinociception), in a nerve injury model of persistent pain.

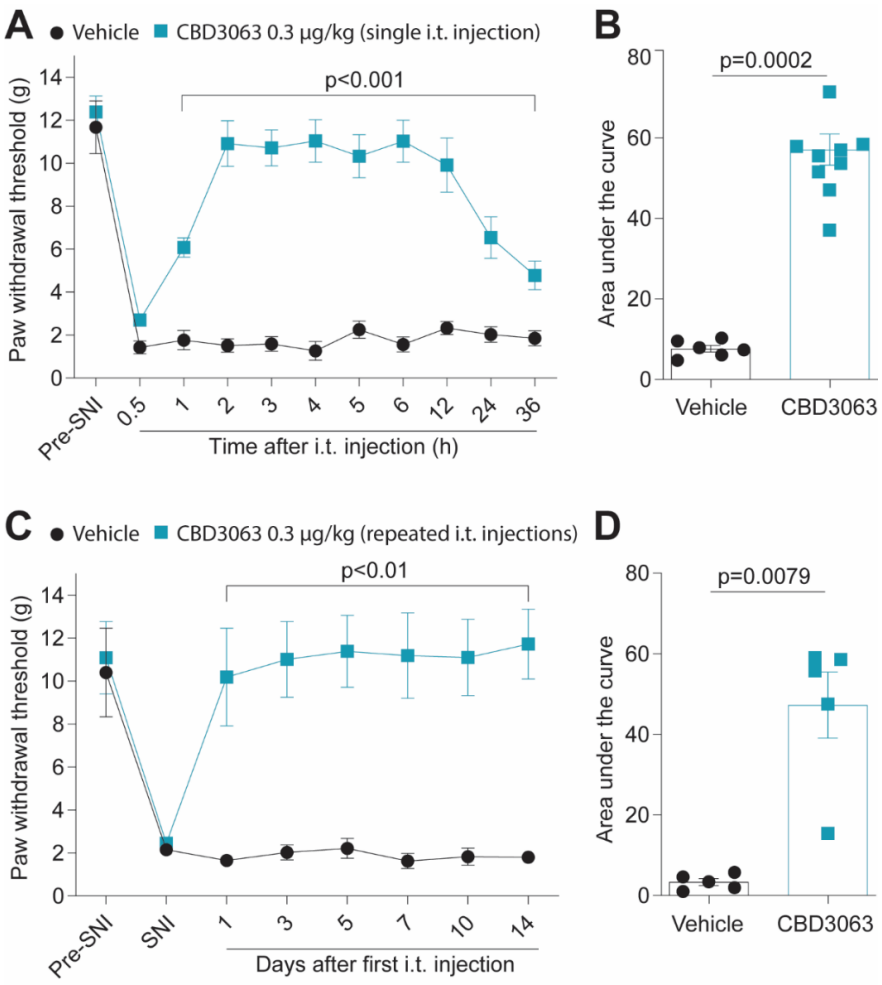

Φιγυρε 8. Σινγλε ανδ ρεπεατεδ ιντρατηεχαλ ινθεστιον οφ ΒΔ3063 (0.3 µγ/κγ) ρεερσε μεχηανιχαλ αλλοδψνια φολλοωινγ σπαρεδ νερε ινθυρψ.(A) Timeline of the experimental paradigm indicating that pre-SNI baseline measurements of withdrawal threshold were taken before nerve injury. A single intrathecal injection of CBD3063 was applied 7 days after SNI, and withdrawal thresholds were followed from 0.5h to 36 hours post injection. p value as indicated; Multiple Mann-Whitney tests. (B) Quantification of the area under the curve between 0.5 and 36 h after i.t. injection. p value as indicated; Mann-Whitney test. N=6-10 rats per conditions; error bars indicate mean ± SEM. (C) Timeline of the repeated i.t. injection of CBD3063 indicating that pre-SNI baseline measurements of withdrawal threshold were taken before nerve injury. After assessing the paw withdrawal threshold 7 days after SNI, intrathecal injections of CBD3063 were applied for 14 consecutive days and paw withdrawal thresholds were assessed at 1, 3, 5, 7 10, and 14 days after the first i.t. injection. p value as indicated; Multiple Mann-Whitney tests. (D) Quantification of the area under the curve between SNI and 14 days after first i.t. injection. p value as indicated; Mann-Whitney test. N=5 rats per group; error bars indicate mean ± SEM.

Discussion

Structure-based drug design allows the optimization of a chemical structure in which the structure of a protein is used as the basis to identify or design new chemical compounds that are predicted to bind to a target (Aparoy, Reddy & Reddanna, 2012). Alternatively, ligand-based approach is used in the absence of the protein structure and relies on knowledge of molecules that bind to the biological target (Aparoy,

Reddy & Reddanna, 2012). To disrupt the $Ca_v2.2$–CRMP2 interaction, we had neither a structure of the complex nor any drug target data. Thus, based solely on the sequence of the CBD3 peptide, we resorted to first principles to identify the structural motif that triggers this interaction. Recently, we tackled a similar problem whereby using MDS, we identified the residue anchoring the interaction between a peptide derived from the disordered N-terminal of $K_v2.1$ and syntaxin1a, which in combination with syntaxin crystal structure led us to the discovery of a first-in-class small molecule neuroprotectant (Yeh et al., 2019).

In this study, we developed a novel pipeline that leverages the computational power of MDS to identify the most stable conformational motif of a peptide, i.e., CBD3, and then used it to develop a pharmacophore model to generate peptidomimetics – a medicinal chemistry approach where parts of the peptide are successively replaced by non-peptide moieties until a non-peptide small molecule is discovered (Perez, 2018). Peptides present desirable medicinal properties like predictable metabolism, good efficacy, safety, and tolerability; however, they are chemically and physically unstable due to rapid proteolysis and inadequate membrane permeability (Fosgerau & Hoffmann, 2015). Notably, editing peptide sequences to develop peptidomimetic analogs creates a promising class of therapeutics that can have inherent advantages, including oral administration, good membrane penetration ability, and enhanced biological activity (Smith, 2015). Considering these strengths, our model predicted first-in-class compounds to disrupt the $Ca_v2.2$–CRMP2 interaction. Specifically, we screened more than 27 million commercially available compounds in the ZINC database using the open access server ZincPharmer and identified 77 suitable compounds for experimental testing. The primary *in vitro*screening identified 9 compounds that inhibit Ca^{+2}influx by more than 50% relative to control. Furthermore, analysis of the shared pharmacophores among the 9 compounds permitted us to predict active chemotypes that when screened against MDS of CRMP2-derived peptides allowed us to fully rationalize active from inactive peptides. The latter provides a strong rationale for our method and its potential application for other targets. From a biological point of view, we show that by disrupting the $Ca_v2.2$–CRMP2 interaction, CBD3063: (i) inhibits Ca^{2+} influx in rat DRG neurons, (ii) decreases the functional activity of N-type Ca^{2+}channels, (iii) reduces membrane expression of $Ca_v2.2$, (iv) does not affect the activity of other voltage-gated ion channels, (v) reduces sensory neuron excitability, and (vi) is antinociceptive in rats with a spared nerve injury model of pain.

$Ca_v2.2$ channels are almost expressed exclusively in neuronal tissue (Nowycky, Fox & Tsien, 1985) and are abundant at presynaptic nerve terminals where they trigger the release of neurotransmitters such as glutamate, calcitonin gene-related peptide, and substance P (Evans, Nicol & Vasko, 1996) via physically interacting with the synaptic release machinery (Zamponi, 2003). For this reason, $Ca_v2.2$ channels are critical determinants of increased neuronal excitability (Yang et al., 2018) and neurotransmission that accompany chronic neuropathic pain (Cizkova et al., 2002). In 2018, the Dolphin laboratory (Nieto-Rostro, Ramgoolam, Pratt, Kulik & Dolphin, 2018) reported a mouse expressing $Ca_v2.2$ channels with an extracellularly accessible hemagglutinin epitope tag engineered into their pore forming $Ca_v2.2$ α1 subunit ($Ca_v2.2$_HA) permitting, for the first time, identification of endogenous $Ca_v2.2$ channels in the plasma membrane of sensory neurons. These mice revealed disease-associated changes in the subcellular distribution of $Ca_v2.2$ in the pain pathway that confirmed the importance of these channels as suitable targets for development of novel pain therapies. Consistent with these findings, the therapeutic potential of targeting $Ca_v2.2$ has been demonstrated in $Ca_v2.2$ deficient mice which have reduced responses to mechanical stimuli, radiant heat, and chemical-induced inflammatory pain (Hatakeyama et al., 2001; Kim et al., 2001) and in nociceptive neurons specifically expressing the exon 37a variant of $Ca_v2.2$ ($Ca_v2.2$e[37a]) mice that display increased N-type Ca^{2+} currents and open channel probability when compared to neurons that only express the exon 37b variant of ($Ca_v2.2$e[37b]) (Bell, Thaler, Castiglioni, Helton & Lipscombe, 2004). In these mice, *in vivo* silencing of $Ca_v2.2$e[37a] prevented the development of mechanical allodynia and thermal hyperalgesia, demonstrating that targeting $Ca_v2.2$e[37a] channels by using splice isoform-specific gene silencing is an effective means for controlling the transmission of thermal and mechanical stimuli in pain conditions.

Despite compelling genetic evidence of the importance of $Ca_v2.2$ in pain, clinical development of N-type Ca^{2+} channel blockers have proven to be challenging. Although modulators of $Ca_v2.2$–α2δ interaction (i.e., Gabapentin and Pregabalin) are recommended as first-line treatment for neuropathic pain (Attal et al.,

2006), they only partially alleviate chronic pain, are implicated in overdose deaths (Kuehn, 2022), and cause a litany of side effects (Zamponi, Striessnig, Koschak & Dolphin, 2015). A $Ca_v2.2$-selective, state-dependent inhibitor – N-triazole oxindole (TROX-1) – was reported by Merck but cardiovascular and motor impairment hampered its further development (Abbadie et al., 2010). Another study reported a sulfonamide-derived, state-dependent inhibitor of $Ca_v2.2$, but this compound was limited by structural liabilities of this class of compounds (Shao et al., 2012). Targeting other interacting partners of $Ca_v2.2$ can also result in reversal of pain symptoms. For example, the β3 auxiliary subunits interact with $Ca_v2.2$ channels (Ludwig, Flockerzi & Hofmann, 1997; Scott et al., 1996) to speed up their activation, increase their membrane localization, and increase neurotransmitter release (Richards, Butcher & Dolphin, 2004; Welling et al., 1993). Expression of β3 protein increases in neuropathic pain (Li et al., 2012) and β3-null mice exhibit suppressed pain responses due to decreased $Ca_v2.2$ currents (Murakami et al., 2002). Consistent with these findings, we reported that targeting the $Ca_v2.2$–β interaction reduces currents through $Ca_v2.2$ channels, inhibits spinal neurotransmission, and alleviates neuropathic pain (Khanna et al., 2019). Collectively, these studies converge on the idea that targeting auxiliary subunits of $Ca_v2.2$ channels is beneficial for pain management. Along these lines, accumulating evidence points to CRMP2 as a new auxiliary subunit of $Ca_v2.2$ channels (Striessnig, 2018).

Over the past decade, we have shown that interrupting the interaction between $Ca_v2.2$ and CRMP2 with CBD3 peptides is efficacious in reversing pain. We reported that disrupting $Ca_v2.2$ –CRMP2 binding with tat-CBD3 or myr-tat-CBD3 peptides does not affect memory, motor functions, or anxiety/depression, and does not produce any addictive behaviors (Brittain et al., 2011b; Francois-Moutal et al., 2015). Likewise, interrupting this interaction has neuroprotective effects (Brittain et al., 2011a; Brustovetsky, Pellman, Yang, Khanna & Brustovetsky, 2014; Ji et al., 2019). Tat-CBD3 (Brittain et al., 2011a; Brustovetsky, Pellman, Yang, Khanna & Brustovetsky, 2014) and R9-CBD3 (Ji et al., 2019) also disrupts the CRMP2–NMDAR interaction. As a result of this, both peptides attenuate NMDAR-mediated currents, have neuroprotective effects against glutamate-induced Ca^{2+} dysregulation (Brittain et al., 2011a; Brustovetsky, Pellman, Yang, Khanna & Brustovetsky, 2014) and protect against neurotoxicity caused the toxic fragment of amyloid-β $(Aβ)_{25\text{-}35}$ (Ji et al., 2019). These studies demonstrate that interfering with $Ca_v2.2$-CRMP2 binding is safe, beneficial, and does not produce unwanted side effects.

We previously reported that a single amino acid point mutant of CBD3 (tat-$CBD3_{A6K}$) decreased R- and T-type Ca^{2+} currents in DRG neurons (Piekarz et al., 2012), and that tat-CBD3 peptide also decreased T-type currents (Piekarz et al., 2012) in sensory neurons. Importantly, in the present study, CBD3063 did not exert an effect on any other voltage-gated calcium channel, which argues for selectivity of our peptidomimetic compound for $Ca_v2.2$. This is in line with our previous observations that the activity of low-voltage-activated Ca^{2+}channels is independent of CRMP2 (Cai, Shan, Zhang, Moutal & Khanna, 2019). We have shown that Cdk5-mediated CRMP2 phosphorylation at residue S522 increases its binding to $Ca_v2.2$, which leads to an increase in calcium influx (Brittain, Wang, Eruvwetere & Khanna, 2012). To discard a potential effect of CBD3063 on CRMP2 phosphorylation, we measured pS522 CRMP2 and found that CBD3063 did not affect this posttranslational modification. This data correlates with our previous findings that interrupting CaV2.2-CRMP2 interaction with myr-tat-CBD3 does not affect CRMP2 phosphorylation (Francois-Moutal et al., 2015). Along the same lines, we investigated the regulation of sodium channels by CBD3063 since we previously described that phosphorylation and SUMOylation of CRMP2 regulates$Na_v1.7$channel trafficking and activity (Dustrude, Moutal, Yang, Wang, Khanna & Khanna, 2016; Dustrude, Perez-Miller, Francois-Moutal, Moutal, Khanna & Khanna, 2017; Dustrude, Wilson, Ju, Xiao & Khanna, 2013). In the present study, we found that CBD3063 does not directly affect currents through sodium channels, or indirectly through an effect on CRMP2 phosphorylation or CRMP2 SUMOylation (data not shown), indicating that this regulation is unaffected by CBD3063 treatment. These data, together with the lack of effect on K^+ currents, suggest that targeting this interaction with CBD3063 does not result in inhibition of other ion channels relevant for pain signaling or in dysregulation of CRMP2 posttranslational modifications.

Despite the documented success of CBD3 peptide in achieving analgesia without side-effects, peptides are nevertheless hampered by (i) short half-life caused by their poor *in vivo* stability (Bruckdorfer, Marder & Albericio, 2004) which may be attributed to the presence of numerous peptidases and excretory mechanisms

that inactivate and clear peptides, and (ii) negligible bioavailability caused by digestive enzymes that are designed to break down amide bonds of proteins and cleave the same bonds in these peptides. To circumvent some of these problems, in the present work we utilized our pharmacophore modelling to generate small molecule peptidomimetics to improve upon the biological activity of the CBD3 peptide by mimicking the chemical features responsible for bioactivity with enhanced drug-like properties. As a result, in contrast to the short-lived actions of CBD3 peptides, the peptidomimetic developed here (i.e., CBD3063) exhibited prolonged antinociceptive profile following a single intrathecal administration as well as long-lasting (>14 days) reversal of mechanical allodynia with repeated intrathecal dosage in rats with chronic neuropathic pain. The latter also points to a lack of tolerance to CBD3063. The prolonged antinociceptive effect of CBD3063 could be attributed to the significant decrease of action potential firing in sensory neurons that could potentially translate into a decrease in spinal cord excitability and neurotransmitter release (not tested here). These findings are congruent with those observed with an adenoviral form of a mutant CBD3 (i.e., AAV6-CBD3$_{A6K}$), which reduced the firing of dorsal horn neurons and reversed mechanical allodynia and thermal hyperalgesia for up to 6 weeks following intraganglionic delivery of the virus in rats with tibial nerve injury (Yu et al., 2019a).

Here, we have presented a translational workflow that uses structural modeling to direct the resolution of protein-protein interactions involving poorly characterized disordered domains, resulting in both mechanistic insights and the identification of an analgesic. This translational workflow led to the discovery of CBD3063 as a first-in-class, CRMP2-based peptidomimetic, which selectively regulates Cav2.2 to achieve analgesia. We note that although CBD3063 exhibits promising drug-likeness (QED score, **Table 1**) it does have marginal predicted blood-brain barrier penetration (BBB score,**Table 1**). To improve to CNS exposure, CBD3063 can be further optimized to lower the topological polar surface area by, for example, modifying and/or removing the acetamide and urea bonds. Another option to increase hydrophobicity is to introduce aromatic group (e.g., in the acetamide area) or to strategically position fluorine atoms to lower capacity of N-H donor (e.g., as 3-fluro-2-aminopyridyl moiety). Overall, we intend to explore targeted changes in CBD3063 to improve its predicted ADME properties while maintaining its current biochemical profile.

Author Information

Co-corresponding authors:

Dr. Carlos J. Camacho, Department of Computational and Systems Biology, University of Pittsburgh, Pittsburgh, PA, 15261, USA. Email:*ccamacho@pitt.edu* or

Dr. Rajesh Khanna, Department of Molecular Pathobiology, College of Dentistry, New York University, 433 First Avenue, 8Thfloor, New York, NY, 10010, USA. Office phone: (520) 271-0433; Email:*rk4272@nyu.edu*

Author Contributions

R.K. and C.J.C. developed the concept of this project. R.K. designed and supervised experiments and advised in data analysis. K.G., C.J.C. and R.K. wrote the manuscript. K.G., A.C.-R., S.L., D.R., P.D., A.C., and A.M., collected and analyzed the data. K.G., A.C.-R., S.L., D.R., performed electrophysiological recordings. A.C. performed calcium imaging experiments. S.P.-M performed docking studies of the compound. H. and P.S.A. synthesized the compound. Y.L. and X.L. performed behavioral experiments. P.D. and A.M. conducted biochemistry and immunohistochemistry studies. U.S. developed the pharmacophore model and performed the virtual screening. All authors had the opportunity to discuss the results and comment on the manuscript.

Funding Sources

This work was supported by National Institutes of Health awards to R.K. (NINDS (NS098772 and NS120663)), and NIDA (DA042852).

Conflict of Interest

The author declares the following competing financial interest(s): R. Khanna is the co-founder of Regulonix LLC, a company developing non-opioids drugs for chronic pain. In addition, R. Khanna has patents US10287334 (Non-narcotic CRMP2 peptides targeting sodium channels for chronic pain) and US10441586 (SUMOylation inhibitors and uses thereof) issued to Regulonix LLC. R. Khanna and A. Moutal are co-founders of ElutheriaTx Inc., a company developing gene therapy approaches for chronic pain.

Declaration of transparency and scientific rigour

This Declaration acknowledges that this paper adheres to the principles for transparent reporting and scientific rigour of preclinical research as stated in the *BJP* guidelines for*Design and Analysis*, and*Animal Experimentation*, and as recommended by funding agencies, publishers and other organisations engaged with supporting research.

Abbreviations

$Ca_v2.2$, N-type voltage-gated calcium channel; Ca_v1, L-type voltage-gated calcium channel; $Ca_v2.1$, P/Q-type voltage-gated calcium channel; $Ca_v2.3$, R-type voltage-gated calcium channel; Ca_v3, T-type voltage-gated calcium channel; CBD3, calcium channel binding domain 3; CRMP2, collapsin response mediator protein 2; DRG, dorsal root ganglia; i.t. intrathecal; MDS, molecular dynamics simulations; HVA, high voltage activated; $Na_v1.7$, voltage-gated sodium channel isoform 7.

References

Abbadie C, McManus OB, Sun SY, Bugianesi RM, Dai G, Haedo RJ*, et al.* (2010). Analgesic effects of a substituted N-triazole oxindole (TROX-1), a state-dependent, voltage-gated calcium channel 2 blocker. J Pharmacol Exp Ther 334**:** 545-555.

Alexander SP, Christopoulos A, Davenport AP, Kelly E, Mathie A, Peters JA*, et al.* (2021). THE CONCISE GUIDE TO PHARMACOLOGY 2021/22: G protein-coupled receptors. British journal of pharmacology 178 Suppl 1**:** S27-s156.

Aparoy P, Reddy KK, & Reddanna P (2012). Structure and ligand based drug design strategies in the development of novel 5- LOX inhibitors. Curr Med Chem 19**:** 3763-3778.

Attal N, Cruccu G, Haanpaa M, Hansson P, Jensen TS, Nurmikko T*, et al.* (2006). EFNS guidelines on pharmacological treatment of neuropathic pain. Eur J Neurol 13**:** 1153-1169.

Basbaum AI, Bautista DM, Scherrer G, & Julius D (2009). Cellular and molecular mechanisms of pain. Cell 139**:** 267-284.

Bauer CS, Rahman W, Tran-van-Minh A, Lujan R, Dickenson AH, & Dolphin AC (2010). The anti-allodynic alpha(2)delta ligand pregabalin inhibits the trafficking of the calcium channel alpha(2)delta-1 subunit to presynaptic terminals in vivo. Biochem Soc Trans 38**:** 525-528.

Bell TJ, Thaler C, Castiglioni AJ, Helton TD, & Lipscombe D (2004). Cell-specific alternative splicing increases calcium channel current density in the pain pathway. Neuron 41**:** 127-138.

Bellampalli SS, Ji Y, Moutal A, Cai S, Wijeratne EMK, Gandini MA*, et al.* (2019). Betulinic acid, derived from the desert lavender Hyptis emoryi, attenuates paclitaxel-, HIV-, and nerve injury-associated peripheral sensory neuropathy via block of N- and T-type calcium channels. Pain 160**:** 117-135.

Bickerton GR, Paolini GV, Besnard J, Muresan S, & Hopkins AL (2012). Quantifying the chemical beauty of drugs. Nat Chem 4**:** 90-98.

Brittain JM, Chen L, Wilson SM, Brustovetsky T, Gao X, Ashpole NM*, et al.* (2011a). Neuroprotection against traumatic brain injury by a peptide derived from the collapsin response mediator protein 2 (CRMP2). J Biol Chem 286**:** 37778-37792.

Brittain JM, Duarte DB, Wilson SM, Zhu W, Ballard C, Johnson PL*, et al.* (2011b). Suppression of inflammatory and neuropathic pain by uncoupling CRMP-2 from the presynaptic Ca(2)(+) channel complex. Nat Med 17**:** 822-829.

Brittain JM, Piekarz AD, Wang Y, Kondo T, Cummins TR, & Khanna R (2009). An atypical role for collapsin response mediator protein 2 (CRMP-2) in neurotransmitter release via interaction with presynaptic voltage-gated calcium channels. J Biol Chem 284**:** 31375-31390.

Brittain JM, Wang Y, Eruvwetere O, & Khanna R (2012). Cdk5-mediated phosphorylation of CRMP-2 enhances its interaction with CaV2.2. FEBS Lett 586**:** 3813-3818.

Bruckdorfer T, Marder O, & Albericio F (2004). From production of peptides in milligram amounts for research to multi-tons quantities for drugs of the future. Curr Pharm Biotechnol 5**:** 29-43.

Brustovetsky T, Pellman JJ, Yang XF, Khanna R, & Brustovetsky N (2014). Collapsin response mediator protein 2 (CRMP2) interacts with N-methyl-D-aspartate (NMDA) receptor and Na+/Ca2+ exchanger and regulates their functional activity. The Journal of biological chemistry 289**:** 7470-7482.

Cai S, Shan Z, Zhang Z, Moutal A, & Khanna R (2019). Activity of T-type calcium channels is independent of CRMP2 in sensory neurons. Channels (Austin) 13**:** 147-152.

Case DA, Ben-Shalom IY, Brozell SR, Cerutti DS, Cheatham TE, III, Cruzeiro VWD*, et al.* (2018). AMBER 2018Univesity of California, San Francisco.

Chaplan SR, Bach FW, Pogrel JW, Chung JM, & Yaksh TL (1994). Quantitative assessment of tactile allodynia in the rat paw. J Neurosci Methods 53**:** 55-63.

Chi XX, Schmutzler BS, Brittain JM, Wang Y, Hingtgen CM, Nicol GD*, et al.* (2009). Regulation of N-type voltage-gated calcium channels (Cav2.2) and transmitter release by collapsin response mediator protein-2 (CRMP-2) in sensory neurons. J Cell Sci 122**:**4351-4362.

Choe W, Messinger RB, Leach E, Eckle VS, Obradovic A, Salajegheh R*, et al.* (2011). TTA-P2 is a potent and selective blocker of T-type calcium channels in rat sensory neurons and a novel antinociceptive agent. Mol Pharmacol 80**:** 900-910.

Cizkova D, Marsala J, Lukacova N, Marsala M, Jergova S, Orendacova J*, et al.* (2002). Localization of N-type Ca2+ channels in the rat spinal cord following chronic constrictive nerve injury. Exp Brain Res 147**:** 456-463.

Decosterd I, & Woolf CJ (2000). Spared nerve injury: an animal model of persistent peripheral neuropathic pain. Pain 87**:** 149-158.

Doggrell SA (2004). Intrathecal ziconotide for refractory pain. Expert Opin Investig Drugs 13**:** 875-877.

Dustrude ET, Moutal A, Yang X, Wang Y, Khanna M, & Khanna R (2016). Hierarchical CRMP2 post-translational modifications control NaV1.7 function. Proc Natl Acad Sci U S A 113**:** E8443-E8452.

Dustrude ET, Perez-Miller S, Francois-Moutal L, Moutal A, Khanna M, & Khanna R (2017). A single structurally conserved SUMOylation site in CRMP2 controls NaV1.7 function. Channels (Austin) 11**:** 316-328.

Dustrude ET, Wilson SM, Ju W, Xiao Y, & Khanna R (2013). CRMP2 protein SUMOylation modulates NaV1.7 channel trafficking. The Journal of biological chemistry 288**:** 24316-24331.

Evans AR, Nicol GD, & Vasko MR (1996). Differential regulation of evoked peptide release by voltage-sensitive calcium channels in rat sensory neurons. Brain Res 712**:** 265-273.

Evoy KE, Peckham AM, Covvey JR, & Tidgewell KJ (2021). Gabapentinoid Pharmacology in the Context of Emerging Misuse Liability. Journal of clinical pharmacology 61 Suppl 2**:** S89-s99.

Feng ZP, Hamid J, Doering C, Bosey GM, Snutch TP, & Zamponi GW (2001). Residue Gly1326 of the N-type calcium channel alpha 1B subunit controls reversibility of omega-conotoxin GVIA and MVIIA block. J Biol Chem 276**:** 15728-15735.

Fischer G, Pan B, Vilceanu D, Hogan QH, & Yu H (2014). Sustained relief of neuropathic pain by AAV-targeted expression of CBD3 peptide in rat dorsal root ganglion. Gene Ther 21**:** 44-51.

Fosgerau K, & Hoffmann T (2015). Peptide therapeutics: current status and future directions. Drug Discov Today 20**:** 122-128.

Francois-Moutal L, Wang Y, Moutal A, Cottier KE, Melemedjian OK, Yang X*, et al.* (2015). A membrane-delimited N-myristoylated CRMP2 peptide aptamer inhibits CaV2.2 trafficking and reverses inflammatory and postoperative pain behaviors. Pain 156**:** 1247-1264.

Giglio CA, Defino HL, da-Silva CA, de-Souza AS, & Del Bel EA (2006). Behavioral and physiological methods for early quantitative assessment of spinal cord injury and prognosis in rats. Braz J Med Biol Res 39**:** 1613-1623.

Gomez K, Tang C, Tan B, Perez-Miller S, Ran D, Loya S*, et al.*(2022). Stereospecific Effects of Benzimidazolonepiperidine Compounds on T-Type Ca(2+) Channels and Pain. ACS Chem Neurosci.

Goshima Y, Nakamura F, Strittmatter P, & Strittmatter SM (1995). Collapsin-induced growth cone collapse mediated by an intracellular protein related to UNC-33. Nature 376**:** 509-514.

Götz AW, Williamson MJ, Xu D, Poole D, Le Grand S, & Walker RC (2012). Routine Microsecond Molecular Dynamics Simulations with AMBER on GPUs. 1. Generalized Born. J Chem Theory Comput 8**:** 1542-1555.

Gupta M, Lee HJ, Barden CJ, & Weaver DF (2019). The Blood-Brain Barrier (BBB) Score. J Med Chem 62**:** 9824-9836.

Hatakeyama S, Wakamori M, Ino M, Miyamoto N, Takahashi E, Yoshinaga T*, et al.* (2001). Differential nociceptive responses in mice lacking the alpha(1B) subunit of N-type Ca(2+) channels. Neuroreport 12**:** 2423-2427.

Heinke B, Balzer E, & Sandkuhler J (2004). Pre- and postsynaptic contributions of voltage-dependent Ca2+ channels to nociceptive transmission in rat spinal lamina I neurons. Eur J Neurosci 19**:**103-111.

Hendrich J, Van Minh AT, Heblich F, Nieto-Rostro M, Watschinger K, Striessnig J*, et al.* (2008). Pharmacological disruption of calcium channel trafficking by the alpha2delta ligand gabapentin. Proceedings of the National Academy of Sciences of the United States of America 105**:** 3628-3633.

Hoppanova L, & Lacinova L (2022). Voltage-dependent CaV3.2 and CaV2.2 channels in nociceptive pathways. Pflugers Arch 474**:** 421-434.

Inagaki N, Chihara K, Arimura N, Menager C, Kawano Y, Matsuo N*, et al.* (2001). CRMP-2 induces axons in cultured hippocampal neurons. Nat Neurosci 4**:** 781-782.

Irwin S, Houde RW, Bennett DR, Hendershot LC, & Seevers MH (1951). The effects of morphine methadone and meperidine on some reflex responses of spinal animals to nociceptive stimulation. J Pharmacol Exp Ther 101**:** 132-143.

Ji Y, Hu Y, Ren J, Khanna R, Yao Y, Chen Y*, et al.* (2019). CRMP2-derived peptide ST2-104 (R9-CBD3) protects SH-SY5Y neuroblastoma cells against Abeta25-35-induced neurotoxicity by inhibiting the pCRMP2/NMDAR2B signaling pathway. Chem Biol Interact 305**:**28-39.

Ju W, Li Q, Allette YM, Ripsch MS, White FA, & Khanna R (2013). Suppression of pain-related behavior in two distinct rodent models of peripheral neuropathy by a homopolyarginine-conjugated CRMP2 peptide. J Neurochem 124**:** 869-879.

Khanna R, Yu J, Yang X, Moutal A, Chefdeville A, Gokhale V*, et al.* (2019). Targeting the CaValpha-CaVbeta interaction yields an antagonist of the N-type CaV2.2 channel with broad antinociceptive efficacy. Pain 160**:** 1644-1661.

Khanna R, Zougman A, & Stanley EF (2007). A proteomic screen for presynaptic terminal N-type calcium channel (CaV2.2) binding partners. J Biochem Mol Biol 40**:** 302-314.

Kim C, Jun K, Lee T, Kim SS, McEnery MW, Chin H*, et al.* (2001). Altered nociceptive response in mice deficient in the alpha(1B) subunit of the voltage-dependent calcium channel. Mol Cell Neurosci 18**:**235-245.

Koes DR, & Camacho CJ (2012). ZINCPharmer: pharmacophore search of the ZINC database. Nucleic Acids Res 40**:** W409-414.

Kozakov D, Clodfelter KH, Vajda S, & Camacho CJ (2005). Optimal clustering for detecting near-native conformations in protein docking. Biophys J 89**:** 867-875.

Kuehn BM (2022). Gabapentin Increasingly Implicated in Overdose Deaths. JAMA 327**:** 2387.

Li L, Cao XH, Chen SR, Han HD, Lopez-Berestein G, Sood AK*, et al.*(2012). Up-regulation of Cavbeta3 subunit in primary sensory neurons increases voltage-activated Ca2+ channel activity and nociceptive input in neuropathic pain. J Biol Chem 287**:** 6002-6013.

Lipinski CA (2004). Lead- and drug-like compounds: the rule-of-five revolution. Drug Discov Today Technol 1**:** 337-341.

Ludwig A, Flockerzi V, & Hofmann F (1997). Regional expression and cellular localization of the alpha1 and beta subunit of high voltage-activated calcium channels in rat brain. J Neurosci 17**:**1339-1349.

Maier JA, Martinez C, Kasavajhala K, Wickstrom L, Hauser KE, & Simmerling C (2015). ff14SB: Improving the Accuracy of Protein Side Chain and Backbone Parameters from ff99SB. J Chem Theory Comput 11**:** 3696-3713.

Mintz IM, Venema VJ, Swiderek KM, Lee TD, Bean BP, & Adams ME (1992). P-type calcium channels blocked by the spider toxin omega-Aga-IVA. Nature 355**:** 827-829.

Moutal A, Li W, Wang Y, Ju W, Luo S, Cai S*, et al.* (2018). Homology-guided mutational analysis reveals the functional requirements for antinociceptive specificity of collapsin response mediator protein 2-derived peptides. Br J Pharmacol 175**:** 2244-2260.

Murakami M, Fleischmann B, De Felipe C, Freichel M, Trost C, Ludwig A*, et al.* (2002). Pain perception in mice lacking the beta3 subunit of voltage-activated calcium channels. J Biol Chem 277**:**40342-40351.

Newcomb R, Szoke B, Palma A, Wang G, Chen X, Hopkins W*, et al.*(1998). Selective peptide antagonist of the class E calcium channel from the venom of the tarantula Hysterocrates gigas. Biochemistry 37**:** 15353-15362.

Nieto-Rostro M, Ramgoolam K, Pratt WS, Kulik A, & Dolphin AC (2018). Ablation of alpha2delta-1 inhibits cell-surface trafficking of endogenous N-type calcium channels in the pain pathway in vivo. Proc Natl Acad Sci U S A 115**:** E12043-E12052.

Nowycky MC, Fox AP, & Tsien RW (1985). Three types of neuronal calcium channel with different calcium agonist sensitivity. Nature 316**:**440-443.

Perez JJ (2018). Designing Peptidomimetics. Curr Top Med Chem 18**:** 566-590.

Piekarz AD, Due MR, Khanna M, Wang B, Ripsch MS, Wang R*, et al.*(2012). CRMP-2 peptide mediated decrease of high and low voltage-activated calcium channels, attenuation of nociceptor excitability, and anti-nociception in a model of AIDS therapy-induced painful peripheral neuropathy. Mol Pain 8**:** 54.

Rajamani D, Thiel S, Vajda S, & Camacho CJ (2004). Anchor residues in protein-protein interactions. Proc Natl Acad Sci U S A 101**:**11287-11292.

Richards MW, Butcher AJ, & Dolphin AC (2004). Ca2+ channel beta-subunits: structural insights AID our understanding. Trends Pharmacol Sci 25**:** 626-632.

Ripsch MS, Ballard CJ, Khanna M, Hurley JH, White FA, & Khanna R (2012). A PEPTIDE UNCOUPLING CRMP-2 FROM THE PRESYNAPTIC Ca(2+) CHANNEL COMPLEX DEMONSTRATES EFFICACY IN ANIMAL MODELS OF MIGRAINE AND AIDS THERAPY-INDUCED NEUROPATHY. Transl Neurosci 3**:** 1-8.

Salomon-Ferrer R, Götz AW, Poole D, Le Grand S, & Walker RC (2013). Routine Microsecond Molecular Dynamics Simulations with AMBER on GPUs. 2. Explicit Solvent Particle Mesh Ewald. J Chem Theory Comput 9**:** 3878-3888.

Scott VE, De Waard M, Liu H, Gurnett CA, Venzke DP, Lennon VA*, et al.* (1996). Beta subunit heterogeneity in N-type Ca2+ channels. J Biol Chem 271**:** 3207-3212.

Shao PP, Ye F, Chakravarty PK, Varughese DJ, Herrington JB, Dai G*, et al.* (2012). Aminopiperidine sulfonamide Cav2.2 channel inhibitors for the treatment of chronic pain. J Med Chem 55**:** 9847-9855.

Smith AJ (2015). New horizons in therapeutic antibody discovery: opportunities and challenges versus small-molecule therapeutics. J Biomol Screen 20**:** 437-453.

Sterling T, & Irwin JJ (2015). ZINC 15–Ligand Discovery for Everyone. J Chem Inf Model 55**:** 2324-2337.

Striessnig J (2018). Getting a handle on Ca(V)2.2 (N-type) voltage-gated Ca(2+) channels. Proc Natl Acad Sci U S A 115**:** 12848-12850.

Sutton KG, Martin DJ, Pinnock RD, Lee K, & Scott RH (2002). Gabapentin inhibits high-threshold calcium channel currents in cultured rat dorsal root ganglion neurones. Br J Pharmacol 135**:** 257-265.

Welling A, Bosse E, Cavalie A, Bottlender R, Ludwig A, Nastainczyk W*, et al.* (1993). Stable co-expression of calcium channel alpha 1, beta and alpha 2/delta subunits in a somatic cell line. J Physiol 471**:** 749-765.

Xie JY, Chew LA, Yang X, Wang Y, Qu C, Wang Y*, et al.* (2016). Sustained relief of ongoing experimental neuropathic pain by a CRMP2 peptide aptamer with low abuse potential. Pain 157**:** 2124-2140.

Yaksh TL, & Rudy TA (1976). Chronic catheterization of the spinal subarachnoid space. Physiol Behav 17**:** 1031-1036.

Yang J, Xie MX, Hu L, Wang XF, Mai JZ, Li YY*, et al.* (2018). Upregulation of N-type calcium channels in the soma of uninjured dorsal root ganglion neurons contributes to neuropathic pain by increasing neuronal excitability following peripheral nerve injury. Brain Behav Immun 71**:** 52-65.

Yeh CY, Ye Z, Moutal A, Gaur S, Henton AM, Kouvaros S*, et al.*(2019). Defining the Kv2.1-syntaxin molecular interaction identifies a first-in-class small molecule neuroprotectant. Proc Natl Acad Sci U S A 116**:** 15696-15705.

Yu H, Shin SM, Xiang H, Chao D, Cai Y, Xu H*, et al.* (2019a). AAV-encoded Ca(V)2.2 peptide aptamer CBD3A6K for primary sensory neuron-targeted treatment of established neuropathic pain. Gene Ther 26**:** 308-323.

Yu J, Moutal A, Dorame A, Bellampalli SS, Chefdeville A, Kanazawa I*, et al.* (2019b). Phosphorylated CRMP2 Regulates Spinal Nociceptive Neurotransmission. Mol Neurobiol 56**:** 5241-5255.

Zamponi GW (2003). Regulation of presynaptic calcium channels by synaptic proteins. J Pharmacol Sci 92**:** 79-83.

Zamponi GW, Striessnig J, Koschak A, & Dolphin AC (2015). The Physiology, Pathology, and Pharmacology of Voltage-Gated Calcium Channels and Their Future Therapeutic Potential. Pharmacological reviews 67**:** 821-870.

Zheng Y, Sethi R, Mangala LS, Taylor C, Goldsmith J, Wang M*, et al.* (2018). Tuning microtubule dynamics to enhance cancer therapy by modulating FER-mediated CRMP2 phosphorylation. Nat Commun 9**:**476.

Table 1. Calculated properties of compounds inhibiting Ca^{+2} influx by more than 50%.

ID	IUPAC Name	Compound class
CBD3018	(Z)-N'-{4-[(3R,5S)-3,5-dimethylpiperidin-1-yl]butyl}-N,N"-dimethylguanidine	Guanidines
CBD3026	ethyl N-benzoyl-(R)-arginine	Guanidines
CBD3033	1-methyl-N-{3-[(5-methylpyridin-2-yl)amino]propyl}-6-oxopyridine-3-carboxamide	2-aminopyridylpropyl-c
CBD3038	8-fluoro-N-{3-[(5-methylpyridin-2-yl)amino]propyl}quinoline-2-carboxamide	2-aminopyridylpropyl-c
CBD3039	2-ethyl-5-isopropyl-N-{3-[(5-methylpyridin-2-yl)amino]propyl}pyrazole-3-carboxamide	2-aminopyridylpropyl-c
CBD3062	1-[(3S)-2-oxoazepan-3-yl]-3-[3-(pyridin-2-ylamino)propyl]urea	2-aminopyridylpropylur
CBD3063	(3R)-3-acetamido-N-[3-(pyridin-2-ylamino)propyl]piperidine-1-carboxamide	2-aminopyridylpropylur
CBD3065	N'-benzyl-N-[3-(3,4-dihydro-1H-isoquinolin-2-yl)propyl]guanidine	Guanidines
CBD3074	N-[3-(1,3-dihydroisoindol-2-yl)propyl]-N'-[(2-methoxyphenyl)methyl]guanidine	Guanidines

Compounds identified as active in calcium imaging (**Figure 2A**). Mw, molecular weight (Da); BBB score, indicates probability of compound having CNS exposure where scores in the range [4-6] correctly predicted 90.3% of CNS drugs (Gupta, Lee, Barden & Weaver, 2019); LogS(7.4), predicted solubility (M) at pH 7.4; cLogP, predicted lipophilicity coefficient in octanol/water; HBD, number of hydrogen-bond donors; HBA, number of hydrogen bond acceptors; RO5, binary (Y/N) assignment of complying with Lipinski rule-of-5 (Lipinski, 2004); NHOH, number of polar NH and OH hydrogens; RotB, number of rotatable bonds; TPSA, topological polar surface area ($Å^2$); QED, Quantitative Estimate of Druglikeness where a score of 1 indicates all properties are favorable (Bickerton, Paolini, Besnard, Muresan & Hopkins, 2012). Properties calculated with RDKit and ChemAxon modules.

Table 2. Gating properties of ionic currents recorded from rat DRG neurons in the presence of CBD3063.

	DMSO	CBD3063
	Total Ca^{2+} currents	Total Ca^{2+} currents
Activation		
$V_{1/2}$	-0.665 ± 1.091 (13)	0.971 ± 2.338 (16)
k	7.429 ± 0.991 (13)	11.004 ± 2.181 (16)
Inactivation		
$V_{1/2}$	-17.081 ± 2.647 (13)	-20.944 ± 3.182 (16)
k	-10.916 ± 2.186 (13)	-14.132 ± 2.880 (16)
	N-type Ca^{2+} currents	N-type Ca^{2+} currents
Activation		
$V_{1/2}$	-5.993 ± 0.680 (12)	-5.275 ± 0.669 (17)
k	5.266 ± 0.570 (12)	5.616 ± 0.566 (17)
Inactivation		
$V_{1/2}$	-28.936 ± 2.206 (12)	-31.129 ± 2.169 (17)
k	-15.101 ± 2.011 (12)	-17.247 ± 2.104 (17)
	L-type Ca^{2+} currents	L-type Ca^{2+} currents
Activation		
$V_{1/2}$	-3.677 ± 0.791 (8)	-2.704 ± 0.710 (7)
k	5.797 ± 0.678 (8)	5.528 ± 0.615 (7)

	DMSO	CBD3063
Inactivation		
$V_{1/2}$	-10.531 ± 0.875 (8)	-10.128 ± 2.133 (7)
k	-4.512 ± 0.848 (8)	-4.961 ± 1.976 (7)
	P/Q-type Ca^{2+} currents	P/Q-type Ca^{2+} currents
Activation		
$V_{1/2}$	-3.703 ± 0.987 (9)	-3.265 ± 0.824 (7)
k	5.375 ± 0.835 (9)	4.186 ± 0.663 (7)
Inactivation		
$V_{1/2}$	-18.283 ± 1.478 (9)	-18.667 ± 1.688 (7)
k	-7.593 ± 1.287 (9)	-9.396 ± 1.470 (7)
	R-type Ca^{2+} currents	R-type Ca^{2+} currents
Activation		
$V_{1/2}$	-8.118 ± 0.842 (7)	-4.098 ± 0.693 (11)
k	6.493 ± 0.736 (7)	7.244 ± 0.579 (11)
Inactivation		
$V_{1/2}$	-23.745 ± 3.57 (7)	-16.840 ± 2.186 (11)
k	-13.155 ± 3.325 (7)	-11.870 ± 1.850 (11)
	T-type Ca^{2+} currents	T-type Ca^{2+} currents
Activation		
$V_{1/2}$	-16.859 ± 0.722 (11)	-10.982 ± 1.992 (10)
k	5.736 ± 0.636 (11)	9.924 ± 1.628 (10)
Inactivation		
$V_{1/2}$	-41.506 ± 1.708 (11)	-35.122 ± 2.752 (10)
k	-9.884 ± 1.585 (11)	-12.929 ± 2.490 (10)
	Na^{+} currents	Na^{+} currents
Activation		
$V_{1/2}$	-23.336 ± 0.663 (9)	-21.738 ± 0.852 (12)
k	3.514 ± 0.576 (9)	4.749 ± 0.744 (12)
Inactivation		
$V_{1/2}$	-37.602 ± 3.112 (9)	-32.552 ± 2.084 (12)
k	-16.081 ± 3.278 (9)	-12.003 ± 1.936 (12)

Values are means ± SEM calculated from fits of the data from the indicated number of individual cells (in parentheses) to the Boltzmann equation; $V_{1/2}$ midpoint potential (mV) for voltage-dependent of activation or inactivation; k , slope factor. These values pertain to Fig. 3, 5, 6 and supplementary figure 5. Data were analyzed with Mann-Whitney test.

DRG, dorsal root ganglia; DMSO, dimethyl sulfoxide.